Jet Quenching in Thin Quark-Gluon Plasmas I: Formalism

M. Gyulassy[a], P. Lévai[a,b], **I. Vitev**[a]

[a] *Department of Physics, Columbia University, New York, NY, 10027, USA*
[b] *KFKI Research Institute for Particle and Nuclear Physics, PO Box 49, Budapest, 1525, Hungary*

July 22, 1999

Abstract

The modification and amplification of the gluon angular distribution produced along with hard jets in nuclear collisions is computed. We consider the limit of a thin quark-gluon plasma, where the number of rescatterings of the jet and gluons is small. The focus is on jet quenching associated with the formation of highly off-shell partons in hard scattering events involving nuclei. The interference between the initial hard radiation amplitude, the multiple induced Gunion-Bertsch radiation amplitudes, and gluon rescattering amplitudes leads to an angular distribution that differs considerably from both the standard DGLAP evolution and from the classical limit parton cascading. The cases of a single and double rescattering are considered in detail, and a systematic method to compute all matrix elements for the general case is developed. A simple power law scaling of the angular distribution with increasing number of rescatterings is found and used for estimates of the fractional energy loss as a function of the plasma thickness.

1 Introduction

One of the new predicted observables in nuclear collisions at RHIC energies ($\sqrt{s} \sim 200$ AGeV) is jet quenching [1]-[5]. While collisional energy loss of a hard jet propagating through quark-gluon plasma has been estimated to be modest [1, 2]: $dE_{coll}/dx \ll 1$ GeV/fm, for accessible plasma temperatures, the induced radiative energy loss, as estimated [3, 4] using the Gunion-Bertsch [6] non-abelian generalization of the Bethe-Heitler formula for QED is expected to be significantly larger with $dE_{rad}/dx >$ few GeV/fm. An uncertainty principle analysis in [7] leads to a simple estimate

$$\frac{dE}{dx} \sim \frac{\langle k_\perp^2 \rangle}{2} \, , \tag{1}$$

where $\langle k_\perp^2 \rangle$ is the mean transverse momentum of the radiated gluons. In Ref. [8] a model for non-abelian energy loss was developed and a class of multiple scattering diagrams lead to $dE/dx \sim 1$ GeV/fm independent of the path length. However, in BDMPS [9] gluon rescattering diagrams in the medium were shown to induce a nonlinear enhancement of the energy loss because $\langle k_\perp^2 \rangle = \mu^2 L/\lambda$. The result for an incident very high energy jet penetrating a plasma of thickness, L, in which the mean free path, $\lambda = 1/(\sigma\rho)$, and the color electric fields are screened on a scale μ, is [9]

$$\frac{dE}{dx} \approx \alpha_s \langle p_\perp^2 \rangle \propto \alpha_s \mu^2 \frac{L}{\lambda} \, . \tag{2}$$

Here $\langle p_\perp^2 \rangle$ is the jet broadening due to multiple elastic scatterings of the jet in matter, and a factor of order unity is suppressed. This estimate is derived for the situation when the radiation formation length is large compared to the target thickness and the target is thick compared to the mean free path:

$$\Delta L_f = E/\mu^2 \gg L \gg \lambda \, .$$

In the other theoretical limit corresponding to Landau–Pomeranchuk–Migdal (LPM) [10] regime in QED, $L \gg \Delta L_f \gg \lambda$, and the energy loss was shown to saturate as $dE/dx \propto \alpha_s \sqrt{\rho E}$.

The remarkable prediction that the non-abelian dE/dx increases linearly with the plasma thickness in nuclear collisions, suggests that the total jet energy loss could increase quadratically with the nuclear size. However, several practical problems limit the application of the above results directly to observable jet quenching in nuclear collisions. First, jets are produced in such reactions with high initial virtualities in hard pQCD processes, and thus induced radiation from secondary interactions must compete with the usual broad gluon shower accompanying a hard pQCD event.

Second, the observable energy loss depends on the detailed angular distribution of the gluons. Unlike in electrodynamics where the energy of the final electron and photon can be directly measured, the energy of a single parton is only measurable when it is kinematically well separated from other jets. This is because the observable hadron showers have wide angular distributions. Nearly collinear partons in particular are not resolvable because they are absorbed into the coherent hadronic wavefunctions. Therefore, in order to test experimentally the non-abelian energy loss of jets, $dN_g/dyd^2\vec{k}_\perp$

of the induced gluon radiation must be known. The angular integrated energy loss, dE/dx, is insufficient to predict its experimental consequences.

Third, for finite nuclei $L/\lambda < 10$ is not very large, and a large fraction of the jets are produced in the nuclear "corona" with $L/\lambda \leq 3$. Thus the form of the angular distribution for only a few collisions is needed.

Fourth, a problem specific to nuclear collisions is that the very large transverse energy background due to minijets (the partons from which the dense quark-gluon plasma is made) prevents the application of traditional transverse energy jet cone measurements of jets [11]. Therefore, jet quenching must be inferred from the systematics of leading hadrons at moderate $p_\perp \sim 3 - 10$ GeV relative to well know spectra in elementary nucleon-nucleon reactions. This step requires the interface of the parton level shower calculations with hadronization phenomenology.

This paper is part I of a study of jet quenching concentrating on the formal problem of computing the angular distribution gluon radiation from off-shell jets produced in a dense but thin medium. In the subsequent paper II [12], we encode the results of this paper into a nuclear collision event generator (HIJING1.36 [13] using the Lund JETSET [14] string fragmentation scheme for hadronization) and compute the hadron inclusive jet quenching pattern. Note that in a separate study [15], the transverse momentum dependence of the LPM effect in QED was discussed in another formalism and compared to the analytic results for QCD derived in this paper.

Multiple interactions in QCD are complicated by the color charge of the radiated gluons. This leads to interference between the production amplitudes and the rescattering amplitudes that makes it impossible to factor the cross section into a product of the elastic cross section and the gluon distribution. In BDMPS, a great technical simplification was achieved by considering only the angular integrated $dN_g/d\omega$, energy distribution. The freedom to shift the transverse momentum, $\vec{k}_\perp$, integrations was used often to reduce the multiple collision problem into tractable form. In addition, a large $n_s = L/\lambda \gg 1$ and $N_c \gg 1$ approximations were employed to convert the problem into an elegant equivalent Schroedinger equation problem valid under the conditions that

$$1/\mu \ll \lambda \ll L \ll L_f = E/\mu^2 \ .$$

An alternative path integral approach proposed in [16] obtained similar results (see also [15]).

Unfortunately, the continuum approximations developed in [17] are not applicable to thin plasmas and more importantly they do not apply at all to the problem of computing the angular distributions. The main complication is that the angular distributions require a complete treatment of all gluon and jet final state interactions. In this paper, we simply follow the direct albeit tedious route of computing the sum of squares of all diagrams with finite number of rescatterings. In the thin plasma limit, the main simplicity arises from the fact that for $n_s \leq 3$ the number of amplitudes $2^{n_s+1} - 1$ is still small enough for practical calculations.

Historically, the on-shell single rescattering case, $n_s = 1$, was first considered by Gunion and Bertsch [6] (GB). They estimated the hadron rapidity distribution due to gluon bremsstrahlung associated with a single elastic valence quark scattering in the Low-Nussinov model. The important difference compared to the problem addressed in

this paper is that GB computed the non-abelian analog of the Bethe-Heitler formula while we are interested in the analog of radiative energy loss in sudden processes similar to the beta decay. The GB problem is to compute the soft radiation associated with a single scattering of an incident on-shell quark prepared in the remote past, i.e., $t_0 = -\infty$, relative to the collision time, t_1. In our case, the radiation associated with a hard jet processes in nuclear reactions must take into account the fact that the jet parton rescatters within a short time , $t_1 - t_0 \sim R_A$, after it is produced. The sudden appearance of the jet color dipole moment within a time interval $\sim 1/E$ results in a broad angular distribution of gluons even with no final state scattering. The induced radiation cased by rescattering necessarily interferes strongly with this hard radiation as indicated in [18].

To model a thin plasma, we employ the static color-screened potential model as considered in Gyulassy–Wang (GW) [8]. The scattering potential has Fourier components

$$V_i \;\; = \;\; V(\vec{q}_i\,)e^{-i\vec{q}_i\cdot\vec{x}_i}\; T_a(R)\otimes T_a(i)\;, \;\; V(\vec{q}_i\,) = \frac{4\pi\alpha_s}{\vec{q}_i^{\,2}+\mu^2}\;. \tag{3}$$

Here $\mathrm{Tr}(T_a(R)T_b(R)) = \delta_{ab}C_R D_R/D_A$ is proportional to the second order Casimir of the D_R dimensional representation R of the jet parton, and $D_A = N_c^2 - 1$. In principle, the i^{th} target could be in the D_i dimensional representation with Casimir $C_2(i)$ so that $\mathrm{Tr}(T_a(i)T_b(j)) = \delta_{ab}\delta_{ij}C_2(i)D_i/D_A$. Note that in eq. (3) V_i corresponds to $A_i(\vec{q}\,)/(-2iP^0)$ in the notation of Ref. [8].

For a thermally equilibrated medium at temperature T, the color screening mass in pQCD is given by $\mu = 4\pi\alpha_s T^2$. In addition, as in ordinary plasmas, no gluon modes propagate below the plasma frequency, $\omega_{pl} \sim \mu/\sqrt{3}$. In practice, lattice QCD calculations of μ indicate sizable nonperturbative corrections to the pQCD estimates for achievable temperatures. Therefore, we simply take here $\mu \sim \omega_{pl} \sim 0.5$ GeV as a characteristic infrared scale of the medium. In perturbation theory, there is a relation between the screening scale μ and the mean free path λ,

$$\mu^2/\lambda \approx 4\pi\alpha_s^2\rho \tag{4}$$

where ρ is the density of plasma partons weighed by appropriate color factors. Another important scale for our problem is the Bethe-Heitler frequency,

$$\omega_{BH} \equiv \frac{1}{2}\mu^2\lambda \gg \mu \tag{5}$$

in the dilute plasma approximation assumed here.

This paper is organized as follows: in Sec. 2 we derive the spectrum of the gluons, radiated as a result of the sudden production of a high energy parton in a highly localized wave-packet $J(p)$ in free space. The large radiative energy loss, which we call "self-quenching", grows as $\Delta E \sim E_0 \log(E_0/\mu)$. The strong destructive interference of this initial amplitude with the subsequent induced radiative and cascade amplitudes is considered in Sec. 3. The main formal results of this paper are derived in that section. In Sec. 3.1 jet acoplanarity is reviewed for the case of multiple elastic scattering

without radiative energy loss. The formal structure of joint jet plus gluon probability density including multiple rescatterings is derived in Sec 3.2. A systematic procedure for extracting all the relevant matrix elements in the eikonal approach is developed using a simple binary encoding scheme in Sec 3.3 to help automate the computation of phase factors and the color algebra. In Sec 3.4 the interference form factors and their dependence on the detailed plasma geometry is derived. These form factors control how close the exact result is to the extreme factorization or the classical parton cascade limits. In Sec. 3.5, the physical interpretation of the relative conditional probabilities computed from the square of the sum of amplitudes and the wavefunction renormalization necessary to compute the gluon angular distribution as a function of n_s is presented. Sec. 4 illustrates in detail the single rescattering case. We rearrange the amplitudes into Gunion-Bertsch and gluon rescattering terms that reduce in special limits to the known cases. An additional form factor associated with the transverse profile of the target is derived that helps to identify the physical interpretation of the rearranged terms. In the simpler "broad" target case, those form factors drop out. The induced gluon bremsstrahlung (beyond self-quenching) is shown to be strongly suppressed relative to the classical limit due to the destructive LPM effect in QCD at small angles. However, the angular enhancement at large angles due to gluon rescattering remains a key feature. The more involved case of two scatterings is treated in Sec. 5. The analytical result shows a power law enhanced angular broadening of the gluon distribution relative to the case of $n_s = 1$. This approximate power law scaling, $\propto (1 + C_A/C_R)^{n_s}$, is used in Sec. 6 to extract an approximate n_s independent reduced quantum modification factor of the gluon angular distribution. We apply this scaling to compute the angular integrated gluon energy spectrum, $dI^{(n_s)}/d\omega$ and the jet fractional energy loss $\Delta E^{(n_s)}/E$. The numerical results show surprisingly an approximate linear dependence of those quantities on the plasma thickness at least up to $L = n_s\lambda \sim 3$ fm. The jet energy loss remains small because the wavefunction renormalization factor also grows rapidly with n_s. As emphasized in the Summary these estimates are only lower bounds because multi-gluon emission is not treated in this paper. The generalization to multi-gluon effects is deferred to ref.[12]. Details of the $n_s = 2, 3$ matrix elements and their rearrangement into the physical hard, Gunion-Bertsch, and gluon cascading components as well as the relevant color factors are recorded in Appendix A and C to ease the flow of the presentation. In Appendix B we compare the $n_s = 2$ case to the approximation of BDMPS where some of the terms in the amplitude were neglected. In Appendix D we derive the curious color "wheel diagram" that arises in the $n_s = 3$ case.

2 Hard Radiation and Self-Quenching

Consider first the amplitude for the production of a hard jet with momentum P_0 localized initially near $x_0^\mu = (t_0, \vec{0})$. We denote this color independent amplitude by

$$\mathcal{M}_J = J(P)e^{iPx_0} \ . \tag{6}$$

The hard vertex is localized within a distance $\sim 1/P_0$, and the amplitude, $J(P)$, is assumed to vary slowly with P on the infrared screening scale μ of the medium. This

spectrum of hard jets is of course softened due to gluon radiation to first order in g_s as shown in Fig. 1.

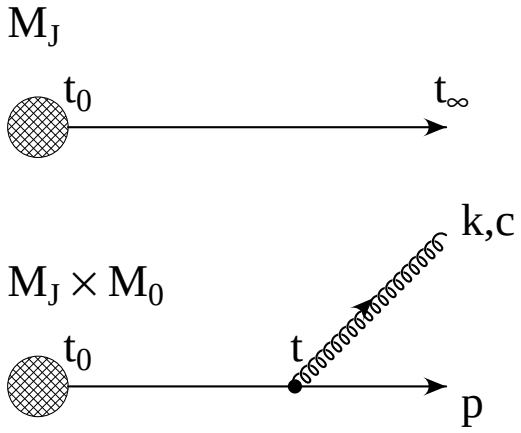

Fig. 1. The M_J hard jet production amplitude and the $M_J \otimes M_0$ soft gluon radiation amplitude.

The final state in that case is characterized by a gluon and a jet with momenta

$$\begin{aligned} k^\mu &= (\omega, k_z, \vec{k}_\perp) = [zP_0^+, \frac{k_\perp^2}{zP_0^+}, \vec{k}_\perp] \, , \\ p^\mu &= (p_0, p_z, \vec{Q}_\perp - \vec{k}_\perp) = [(1-z)P_0^+, \frac{(\vec{Q}_\perp - \vec{k}_\perp)^2}{(1-z)P_0^+}, \vec{Q}_\perp - \vec{k}_\perp] \, , \end{aligned} \tag{7}$$

where $(\cdots)$ denote their 4-momentum and $[\cdots]$ denote their light-cone momentum coordinates.

We emphasize that the "z" direction in this paper refers to the unperturbed hard jet direction. In nuclear reaction, the jets are directed perpendicular to the beam axis in the frame in which its longitudinal rapidity vanishes. Therefore k_x, k_y, k_z actually correspond to a 90 degree rotation about the y axis of the conventional frame in which the z axis is parallel to the beam. The initial "transverse" momentum $\vec{Q}_\perp$ of the jet thus accounts for both its longitudinal rapidity as well as its azimuthal (symmetric) dependence about the beam. The energy loss, ω, leads to a suppression of the high $p_\perp$ distribution of the fragments emerging from the jet.

The gluon polarization in the $A^+ = 0$ gauge is $\epsilon(k) = [0, (2\vec{\epsilon}_\perp \cdot \vec{k}_\perp)/(zP_0^+), \vec{\epsilon}_\perp]$. We consider here eikonal kinematics where

$$\begin{aligned} \omega &= \sqrt{k_z^2 + k_\perp^2} \approx zE_0 + \frac{k_\perp^2}{2zE_0} \, , \\ p^0 &= \sqrt{p_z^2 + p_\perp^2} \approx (1-z)E_0 + \frac{(\vec{Q}_\perp - \vec{k}_\perp)^2}{2(1-z)E_0} \, . \end{aligned} \tag{8}$$

The amplitude to emit a soft gluon and the jet neglecting spin effects can be expressed as

$$\mathcal{M}_J \otimes \mathcal{M}_0 = i \int d^4P \; J(P) e^{iPx_0} \frac{(-ig_s T_c) \; \epsilon \cdot (2p+k)}{(p+k)^2} \delta^4(P-k-p) \approx$$

$$\approx \quad e^{iE_0 t_0} J(k+p)\mathcal{M}_0(k,p) \; , \tag{9}$$

where $\mathcal{M}_0$ is the radiation amplitude that in the eikonal limit is given by

$$\mathcal{M}_0 \quad = \quad -2ig_s \frac{\vec{\epsilon}_\perp \cdot \vec{k}_\perp}{k_\perp^2} e^{it_0 \frac{k_\perp^2}{2\omega}} c \; . \tag{10}$$

Here, $c \equiv T_c(R)$ is the $SU(N_c)$ color generator T_c in the D_R dimensional representation of the jet parton with $Tr(cc) = C_R D_R$.

A simple direct way to recover the phase factor and the $1/k_\perp^2$ singularity of $\mathcal{M}_0$ is through the use time ordered perturbation theory as emphasized in [9]. This follows from integrating over the emission time of the gluon

$$\int_{t_0}^{\infty} dt \; e^{-\varepsilon|t| + i(E_f - E_i)t} = \frac{2\omega}{k_\perp^2} e^{it_0 \frac{k_\perp^2}{2\omega}} \; , \tag{11}$$

where

$$E_f - E_i = \omega + p_0 - E_0 \approx k_\perp^2 / 2\omega \; .$$

This method is particularly useful when final state interactions are taken into account in the next sections.

The probability distribution for the jet production is given by

$$d^3\mathcal{D}^{(0)} = D_R |\mathcal{M}_J|^2 \frac{d^3\vec{p}}{(2\pi)^3 2p^0} \equiv \rho^{(0)}(\vec{p}) \frac{d^3\vec{p}}{(2\pi)^3 2|\vec{p}|} \; , \tag{12}$$

where $\rho^{(0)}(p)$ is proportional to the invariant hard production probability density with no elastic rescatterings of the jet nor radiative energy loss. The pQCD jet distribution is approximately a power law $1/p_\perp^{2q}$ relative to the beam axis and uniformly distributed in longitudinal rapidity. The power $q \sim 3$ depending on the beam energy and the $p_\perp$ range under consideration. However, in terms of our rotated variables with $p_z \leftrightarrow p_x$

$$\rho^{(0)}(\vec{p}) \sim c/(p_z^2 + p_y^2)^q$$

independent of our p_x that is parallel to the beam direction. We emphasize this point because unlike the usual energy loss problem of a beam passing through matter, the peculiar longitudinally expanding cylindrical geometry of the matter in nucleus collisions makes applications of simple formulas in the rotated frame somewhat unintuitive.

The double inclusive jet plus gluon probability distribution is given by

$$d^6\mathcal{D}^{(0)}_{rad} = \rho^{(0)}_{rad}(k,p) \frac{d^3\vec{k}}{(2\pi)^3 2\omega} \frac{d^3\vec{p}}{(2\pi)^3 2p^0} \; , \tag{13}$$

where

$$\rho^{(0)}_{rad}(k,p) \equiv \mathrm{Tr}|\mathcal{M}_J \otimes \mathcal{M}_0|^2 \tag{14}$$

is the double inclusive probability density for producing a jet and a gluon in the case of no rescatterings.

As seen from (9,10) the double inclusive density factorizes for soft gluons into a production probability of an off-shell jet with $k+p$ and a distribution of gluons.

$$\omega\frac{d^3N_g^{(0)}}{d^3\vec{k}} \approx \frac{C_R\alpha_s}{\pi^2}\frac{1}{k_\perp^2} \equiv R_g^{(0)}(\vec{k}) \ , \tag{15}$$

where the dependence on p is only implicit through the kinematic boundaries. As in QED the radiation pattern associated with a hard jet corresponds to a uniform rapidity distribution along the jet axis with a broad transverse transverse momentum distribution that is uniform in $\log k_\perp^2$.

If the off-shell dependence of the source amplitude is weak and the gluon is soft in the sense

$$\frac{1}{|\vec{p}|}|J(|\vec{p}|+\omega,\vec{p}+\vec{k}\,)|^2 \approx \frac{1}{|\vec{p}+\vec{k}|}|J(|\vec{p}+\vec{k}|,\vec{p}+\vec{k})|^2 \ ,$$

then we can write

$$\rho_{rad}^{(0)}(\vec{k},\vec{p}) \approx 2(2\pi)^3\rho^{(0)}(\vec{p}+\vec{k})R^{(0)}(\vec{k}) \ . \tag{16}$$

The gluon radiation associated with any hard pQCD process leads to what one can think of as "self-quenching" of the jet in the sense that the initially produced high energy jet parton loses a substantial fraction of its energy

$$\Delta E_0 = C_R\frac{\alpha_s}{\pi}\int_0^1\frac{dz}{z}\int_{\mu^2}^{E^2}\frac{dk_\perp^2}{k_\perp^2}\,zE_0 \sim C_R\frac{2\alpha_s}{\pi}E_0\ \log(E_0/\mu) \ . \tag{17}$$

This occurs even in free space where there are no final state interactions. In practice, the large logarithm implies that multiple gluon emission must also be considered. This leads to a Sudakov form factor for the jet and a probabilistic Alterelli-Parisi parton shower [19]. The final state multigluon shower can be calculated most readily by one of the many Monte–Carlo event generators such as PYTHIA [20]. Those generators encode empirical "parton to hadron" fragmentation functions and thus allow the detailed study of the effect of parton showering on the final hadron distributions. The magnitude of the self-quenching effect, i.e., initial and final state radiation, is found to be significant and is essential to describe accurately the high $p_\perp$ data as shown in [21]. Our main interest here is to derive the extra quenching associated with gluon radiation induced by final state interactions of the jet in a thin plasma.

3 Gluon Radiation with Rescatterings

In this section, the self-quenching case is generalized to take into account possible multiple scattering of the jet and gluon following the hard jet production.

3.1 Multiple Elastic Scattering

The amplitude that jet undergoes n_s elastic scatterings with momentum transfers $q_i = (0,q_{iz},\vec{q}_{i\perp})$ is given by [8]

$$\mathcal{M}_J^{(n_s)} \ = \ \int d^4P\ J(P)e^{iPx_0}\int\prod_{i=1}^{n_s}\left(\frac{d^3\vec{q}_i}{(2\pi)^3}\ (2P^0T_{a_i}(i)\Delta(P+Q_{i-1})V(\vec{q}_i)e^{-i\vec{q}_i\vec{x}_i}\right)$$

$$\times\, \delta^4(P-p+\sum q_i)\left(T_{a_1}(R)\cdots T_{a_{n_s}}(R)\right)\ . \tag{18}$$

where $\Delta(p)=(p^2-m^2+i\epsilon)^{-1}$ is the jet propagator neglecting spin effects, and the cumulative momentum transfer $Q_i\equiv\sum_{j=1}^{i}q_j$. The invariant jet probability distribution together with n_s unobserved recoil partons in the target and no gluon radiation is to lowest order (without Sudakov factor) given by

$$d^3\mathcal{D}_{el}^{(n_s)}=\left\langle\ \mathrm{Tr}|\mathcal{M}_J^{(n_s)}|^2\ \right\rangle_{\vec{x}}\frac{d^3\vec{p}}{(2\pi)^3 2p^0}=\rho_{el}^{(n_s)}(p)\frac{d^3\vec{p}}{(2\pi)^3 2p^0}\ . \tag{19}$$

The ensemble average over the location of the scattering centers is taken as in [8]

$$\langle\cdots\rangle_{\vec{x}}=\int\prod_{i=1}^{n_s}\left(d\vec{x}_{i\perp}T(\vec{x}_{i\perp})\int_0^\infty\frac{d(z_i-z_{i-1})}{\lambda_i}e^{-\frac{z_i-z_{i-1}}{\lambda_i}}\theta(z_i-z_{i-1})\right)(\cdots)\ . \tag{20}$$

In a static medium, the average longitudinal separation between the centers is specified by the mean free path, $\lambda=\lambda_i$. An expanding medium, on the other hand, has $\lambda_i>\lambda_{i-1}$ can only be approximately treated with a constant mean free path. The transverse coordinates are distributed according to a normalized overlap function, $T(\vec{x}_\perp)\sim 1/(\pi R_\perp^2)$. We assume that the transverse size $R_\perp$ of the target (relative to the jet axis) is large compared to the range of the interactions, $1/\mu$.

In the high energy ($p^0=E\gg\omega\gg\mu$) eikonal limit, going back to the picture including the momenta of the jet, the integrations over p_{iz} are fixed by residues approximately to $p_{iz}\approx E-p_{i\perp}^2/(2E)$. The contributions from the poles of the static potential are suppressed by a factor $\propto exp(-\mu\lambda)$. In this model we neglect the small collisional energy loss associated with target: $dE_{el}/dx\approx 4\alpha_s^2T^2\log E/\mu\sim 0.3$ GeV/fm [1, 2].

Elastic scattering modifies the jet distribution in eq. (19) in this eikonal limit as

$$\begin{aligned}\rho_{el}^{(n_s)}(p)\ &\approx\ \int\prod_{i=1}^{n_s}\left(\frac{d^2\vec{q}_i}{(2\pi)^2}\frac{d^2\vec{q}_i{}'}{(2\pi)^2}\,V(\vec{q}_i)V^*(\vec{q}_i{}')\frac{C_RC_2(i)}{D_A}T(\vec{q}_{i\perp}-\vec{q}_{i\perp}')\right)\\ &\quad\times(D_RJ(p-Q)J^*(p-Q'))\\ &\approx\ \int\frac{d^2\vec{Q}_\perp}{(2\pi)^2}\rho^{(0)}(p-Q)\int\prod_{i=1}^{n_s}\left(d^2\vec{q}_i\frac{d^2\sigma_{el}}{d^2\vec{q}_{i\perp}}\right)\left(\frac{d^2\vec{q}_i{}'}{(2\pi)^2}T(\vec{q}_i{}')\right)\\ &\quad\times(2\pi)^2\delta^2(\vec{Q}_\perp-\sum_{j=1}^{n_s}\vec{q}_{i\perp})\ ,\end{aligned} \tag{21}$$

which includes the expected jet acoplanarity [22, 23] resulting from random walk but no recoil energy loss.

The major simplification in the above derivation arises from the assumption that $|\vec{q}_i-\vec{q}_i{}'|\sim 1/R_\perp\ll\mu\ll\lambda$ so that the main source of non-diagonal dependence arises through the $T(\vec{q}_{i\perp}-\vec{q}_{i\perp}')$ factors. This is what allows us to recover the above classical elastic parton cascade form in terms of the effective differential cross sections

$$\frac{d^2\sigma_{el}}{d^2\vec{q}_{i\perp}}=\frac{C_RC_2(i)}{D_A}\frac{4\alpha_s^2}{(q_{i\perp}^2+\mu^2)^2}\ . \tag{22}$$

The elastic cross section is then $\sigma_{el} = (C_R C_2(i)/D_A)(4\pi\alpha_s^2/\mu^2)$ which for a glue jet propagating in a glue plasma with $\mu = 0.5$ GeV is typically $\sigma_{el} \sim 2$ mb. (See Ref. [24] for a new Monte–Carlo implementation of such an elastic parton cascade.)

We will neglect the influence of elastic multiple scattering on the inclusive distribution of jets because $\rho^{(0)}(p)$ is broadly distributed and the elastic energy loss is relatively small. In this case, $\rho^{(0)}(p-Q) \approx \rho^{(0)}(p)$ can be factored out of eq. (21) leading to

$$\rho_{el}^{(n_s)}(p) \;\approx\; \rho^{(0)}(p)\,(\sigma_{el}T(0))^{n_s}\;, \tag{23}$$

which is simply proportional to the free space spectrum times a geometrical factor (the Glauber multiple collision probability).

3.2 Gluon Radiation with Quantum Cascading

The amplitude to emit a gluon together with the jet including final state interactions with n_s scattering centers is given by

$$\begin{aligned}\mathcal{M}_J^{(n_s)} \otimes \mathcal{M}_{n_s} \;&=\; \int d^4P\; J(P)e^{iPx_0}\int\prod_{i=1}^{n_s}\left(\frac{d^3\vec{q}_i}{(2\pi)^3}\,(-2iP^0)V(\vec{q}_i)e^{-i\vec{q}_i\vec{x}_i}T(i)\right)\\ &\quad\times\mathcal{M}_{n_s}(k,p;q_1,\cdots,q_{n_s})\;\delta^4(P-k-p+\textstyle\sum q_i)\;.\end{aligned} \tag{24}$$

This leads to the conditional double inclusive jet and gluon probability distribution

$$d^6\mathcal{D}_{rad}^{(n_s)} = \rho_{rad}^{(n_s)}(k,p)\frac{d^3\vec{k}}{(2\pi)^3 2\omega}\frac{d^3\vec{p}}{(2\pi)^3 2p_0}\;,$$

$$\rho_{rad}^{(n_s)}(k,p) = \left\langle|\mathcal{M}_J^{(n_s)}\otimes\mathcal{M}_{n_s}|^2\right\rangle \equiv (\prod_{i=1}^{n_s}\frac{1}{D_i})\mathrm{Tr}\left\langle|\mathcal{M}_J^{(n_s)}\otimes\mathcal{M}_{n_s}|^2\right\rangle_{\vec{x}}\;, \tag{25}$$

which involves averaging over all initial target colors and summing over all final colors and the locations $\vec{x}_i$ of the target centers.

After integrating over the energy-conserving delta functions we arrive at the momentum space distribution density

$$\begin{aligned}\rho_{rad}^{(n_s)}(k,p) \;&=\; \int\prod_{i=1}^{n_s}\left(\frac{d^3\vec{q}_i}{(2\pi)^3}\,\frac{d^3\vec{q}_i{}'}{(2\pi)^3}\,(2p^0)^2V(\vec{q}_i)V^*(\vec{q}_i{}')(C_2(i)/D_A)\right)\\ &\quad\times\left\langle\;\prod_{i=1}^{n_s}e^{-i(\vec{q}_i-\vec{q}_i{}')\vec{x}_i}\;\right\rangle_{\vec{x}} J(k+p-\textstyle\sum q_i)J^*(k+p-\sum q_i{}')\\ &\quad\times\mathrm{Tr}\left(\mathcal{M}_{n_s}(k,p;q_1,\cdots,q_{n_s})\mathcal{M}_{n_s}^\dagger(k,p;q_1',\cdots,q_{n_s}')\right)\;.\end{aligned} \tag{26}$$

The amplitude $\mathcal{M}_{n_S}$ is a sum over all time-ordered graphs involving n_s scatterings in which one gluon is radiated.

For a slowly varying source, $J(p+k-Q) \approx J(p+k)$ can be factored out of the integral in eq. (26) leading to

$$\begin{aligned}\rho_{rad}^{(n_s)}(k,p) &\approx |J(p+k)|^2 \int \prod_{i=1}^{n_s} \left(\frac{d^3\vec{q}_i}{(2\pi)^3} \frac{d^3\vec{q}_i'}{(2\pi)^3} V(\vec{q}_i) V^*(\vec{q}_i') \frac{(2p^0)^2 C_2(i)}{D_A} T(\vec{q}_{i\perp} - \vec{q}_{i\perp}') \right) \\ &\times \left\langle \prod_{i=1}^{n_s} e^{-i(q_{iz}-q_{iz}')z_i} \right\rangle_z \\ &\times \mathrm{Tr}\left(\mathcal{M}_{n_s}(k,p;q_1,\cdots,q_{n_s}) \mathcal{M}_{n_s}^\dagger(k,p;q_1',\cdots,q_{n_s}') \right) \ . \end{aligned} \tag{27}$$

The integration over the q_{iz} can again be performed by contour integration leading to a sum over many terms with longitudinal phases set by energy differences as in [8, 9]. In the eikonal limit, a simple shortcut to that calculation is possible when the scattering of potentials localized in the longitudinal direction at z_i can be approximated by impulse interactions at times, $t_i \approx z_i/c$ [9]. In that case, time ordered perturbation theory can be used to express eq. (27) as

$$\begin{aligned}\rho_{rad}^{(n_s)}(k,p) &\approx |J(p+k)|^2 \int \prod_{i=1}^{n_s} \left(\frac{d^2\vec{q}_i}{(2\pi)^2} \frac{d^2\vec{q}_i'}{(2\pi)^2} V(\vec{q}_i) V^*(\vec{q}_i') \frac{C_2(i)}{D_A} T(\vec{q}_{i\perp} - \vec{q}_{i\perp}') \right) \\ &\times \left\langle \mathrm{Tr}\left[\left(\sum_{m=0}^{n_s} \sum_{l=1}^{2^m} \mathcal{M}_{n_s,m,l}(k,p;\vec{q}_{1\perp},\cdots,\vec{q}_{n_s\perp}) \right) \right. \right. \\ &\times \left. \left. \left(\sum_{m'=0}^{n_s} \sum_{l'=1}^{2^{m'}} \mathcal{M}_{n_s,m',l'}^\dagger(k,p;\vec{q}_{1\perp}',\cdots,\vec{q}_{n_s\perp}') \right) \right] \right\rangle_t \ , \end{aligned} \tag{28}$$

where the sums go over the $2^{n_s+1}-1$ different time ordered diagrams that we list in the next sections. The reduced radiation amplitudes, $\mathcal{M}_{n_s,m,l}$, for a given n_s are labeled by two integers, $0 \le m \le n_s$ and $0 \le l$. Here m specifies the time interval $t_m < t < t_{m+1}$ in which the gluon is radiated and l specifies which of the 2^{n_s-m} final state interaction patterns with centers $m+1,\cdots,n_s$ occurs.

3.3 Reduced Radiative Amplitudes

It is convenient to associate with each amplitude diagram, $\mathcal{M}_{n_s,m,l}$, an n_s dimensional binary array, $\vec{\sigma}$, that decodes the label l for a given m as follows:

$$\vec{\sigma} = (\sigma_1 = 0, \cdots, \sigma_m = 0, \sigma_{m+1}, \cdots, \sigma_{n_s})_m \Longleftrightarrow l = (\sum_{j=1}^{n_s} \sigma_j 2^j)/2^{m+1} \ , \tag{29}$$

where $\sigma_i = 0$ for $1 \le i \le m$ while $\sigma_i = 0$ or 1 for $m+1 \le i \le n_s$ depending on the integer part of $l/2^{i-m-1}$. This is the base 2 representation of $l \times 2^{m+1} = \sigma_{n_s} \cdots \sigma_1$ so that $0 \le l \le 2^{n_s-m} - 1$. For a fixed m, $l = 0$ corresponds then to no final state gluon rescattering, while $l = 2^{n_s-m} - 1$ corresponds to the gluon rescattering with all $n_s - m$ remaining scattering centers after t_m.

For example, Fig. 2 shows $\mathcal{M}_{5,1,10}$ as the time ordered diagram with $n_s = 5$ scattering centers, where gluon was emitted from the jet between t_1 and t_2 and $l = 10$ corresponding to $\vec{\sigma} = (0, 0, 1, 0, 1)$ encodes the fact that the gluon received impulses $\vec{q}_{\perp 3}, \vec{q}_{\perp 5}$ at times, t_3 and t_5.

The binary representation is useful as a mask to extract the correct kinematic variables automatically. The transverse momentum of the gluon between interactions i and $i + 1$ is simply

$$\vec{K}_i = \vec{k}_\perp - \sum_{j=i+1}^{n_s} \sigma_j \vec{q}_{j\perp} = \vec{K}_{i-1} + \sigma_i \vec{q}_{i\perp} \ , \tag{30}$$

with $\vec{K}_{n_s} \equiv \vec{k}_\perp$, the final gluon transverse momentum. For the example in Fig. 2, $\vec{K}_0 = \vec{K}_1 = \vec{K}_2 = \vec{k}_\perp - \vec{q}_{3\perp} - \vec{q}_{5\perp}$ and $\vec{K}_3 = \vec{K}_4 = \vec{k}_\perp - \vec{q}_{5\perp}$.

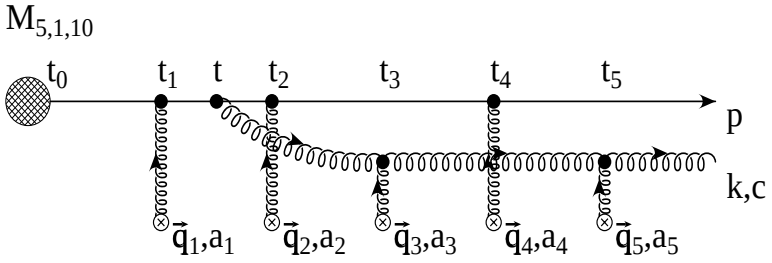

Fig. 2. Example of the reduced $\mathrm{M}_{5,1,10}$ radiative amplitude for $n_s = 5$.

The complete amplitude matrix can be constructed in a few steps. First, the time integration over the emission times between t_m and t_{m+1} and the n_s impulses gives rise to the factor

$$\frac{\omega}{\omega_{ml}} \left(e^{i\omega_{ml} t_{m+1}} - e^{i\omega_{ml} t_m} \right) e^{i\Phi_{lm}} \ , \tag{31}$$

where the energy shift at the emission point is denoted

$$\omega_{ml} = \frac{K_m^2}{2\omega} = \frac{\left(\vec{k}_\perp - \sum_{j=1}^{n_s} \sigma_j \vec{q}_{j\perp} \right)^2}{2\omega} \ . \tag{32}$$

The apparent singularity at $\omega_{ml} = 0 = K_m^2$ due to the energy denominator is cancelled for finite $t_{m+1} - t_m < \infty$. The singular $t_{n_s+1} = \infty$ phase is always suppressed by an adiabatic damping factor (not shown). The only singular amplitude is in fact, the one corresponding to the factorization limit in which final state interactions factor out. Including the eikonal gluon emission vertex $2ig_s \epsilon_\mu(K_m) p^\mu \approx g_s \vec{\epsilon}_\perp \cdot \vec{K}_m$, the special case for $m = n_s$, $l = 0$ reduces to

$$\mathcal{M}_{n_s,n_s,0} = -2ig_s \frac{\vec{\epsilon}_\perp \cdot \vec{K}_{n_s}}{K_{n_s}^2} e^{it_{n_s} \frac{K_{n_s}^2}{2\omega}} c(a_{n_s} \cdots a_1) = e^{i(t_{n_s} - t_0) \frac{k_\perp^2}{2\omega}} \mathcal{M}_0 \left(a_{n_s} \cdots a_1 \right) \ ,$$

where $\mathcal{M}_0$ is given by eq. (10). All the other amplitudes remain bounded $|\mathcal{M}_{n_s,m,l}| < C(t_{m+1} - t_m)$. On the other hand, in the formal $t_0 \to -\infty$ limit, all the $2^{n_s} - 1$ singularities at $\omega_{ml} = 0$ become exposed.

The overall eikonal phase, Φ_{ml}, acquired by the gluon through final state interactions is

$$\Phi_{ml} \;=\; \sum_{j=1}^{n_s} \Omega_{mlj} t_j = \sum_{j=1}^{n_s} \frac{t_j}{2\omega}\left(\vec{K}_j^{\,2} - \vec{K}_{j-1}^{\,2}\right) = \sum_{j=m+1}^{n_s} \sigma_j \frac{t_j}{2\omega}\left(\vec{K}_j^{\,2} - (\vec{K}_j - \vec{q}_{j\perp})^2\right) \;, \quad (33)$$

where $\Omega_{mlj} = \partial\Phi_{ml}/\partial t_j$.

The amplitude for color exchange leaving the final gluon with color $c = 1, \cdots, D_A$ is specified by a particular color matrix, T_{mlc}. The scattering of the jet with center i brings in a color matrix $a_i \equiv T_{a_i}(R)$ in the R representation. Gluons interact with center i, on the other hand with $T_{a_i}(A)$ in the adjoint representation. It is numerically convenient, however, to express the complete color structure involving gluon final state interactions in terms of commutators in the jet (R dim) representation. Label sequentially in increasing order all $n_g = \sum_k \sigma_k$ color matrices, a_k where $\sigma_k = 1$, by $c_1, \cdots, c_{n_g}$. Label all remaining $n_s - m - n_g$ matrices with $k > m$ and $\sigma_k = 0$ by $b_1, \cdots, b_{n_s-m-n_g}$. Then

$$T_{mlc} = \left(b_{n_s-m-n_g} \cdots b_1\right)\Big[\cdots[c, c_{n_g}], \cdots, c_1\Big]\left(a_m \cdots a_1\right) \;. \quad (34)$$

In the example of Fig. 2, $T_{1,10,c} = a_4 a_2 [[c, a_5], a_3] a_1$. Eq. (34) defines a straightforward algorithm for numerical computation of color factors,

$$C_{mlm'l'} = \sum_{c,a_1,\cdots,a_n} \mathrm{Tr}\,\left(T_{mlc} T^{\dagger}_{m'l'c}\right) ,$$

needed as weights of the different interference terms in eq. (28) .

Finally, the reduced radiation amplitudes with final state interactions are given by

$$\mathcal{M}_{n_s,m,l} = 2ig_s \frac{\vec{\epsilon}_\perp \cdot \vec{K}_m}{K_m^2}\left(e^{i\frac{t_{m+1}K_m^2}{2\omega}} - e^{i\frac{t_m K_m^2}{2\omega}}\right) e^{i\Phi_{lm}} T_{mlc} \;. \quad (35)$$

3.4 Interference Form Factors

If the "width", $R_\perp \gg \lambda \gg 1/\mu$, of the target transverse to the jet direction is large compared to its thickness, L, (i.e., $R_\perp \gg L > \lambda \gg 1/\mu$), then the off diagonal dependence in $|\vec{q}_{i\perp} - \vec{q}\,'_{i\perp}| \sim 1/R_\perp$ in eq. (28) can be ignored in all factors except $T(\vec{q}_{i\perp} - \vec{q}\,'_{i\perp})$ (see Sec. 4.1 for more detailed discussion on this). In this case, the interference terms arising from the distribution of scattering times, t_i, involve the following form factors:

$$F_{mlm'l'} \equiv \left\langle\; e^{i(\Phi_{ml} - \Phi_{m'l'})}\left(e^{it_{m+1}\omega_{ml}} - e^{it_m\omega_{ml}}\right)\left(e^{-it_{m'+1}\omega_{m'l'}} - e^{-it_{m'}\omega_{m'l'}}\right)\right\rangle \;. \quad (36)$$

For $m, m' < n_s$, the form factors insure that $F_{mlm'l'}/(\omega_{ml}\omega_{m'l'})$ have no singularities except for $m, m' = n_s$, and control the magnitude of the destructive LPM interference effects. The diagonal form factors are given by

$$F_{mlml} \;=\; 2 - 2\left\langle\, \cos((t_{m+1} - t_m)\omega_{ml})\,\right\rangle \;, \quad (37)$$

except that $F_{n_s 0 n_s 0} = 1$ since $t_{n_s+1} = \infty + i\epsilon$. The extreme limits of quantum cascading correspond to (1) the incoherent Classical Parton Cascade limit and (2) the coherent Factorization limit. In the first case, all non-diagonal form factors vanish, while in the second case all but the $m = n_s$ diagonal form factor vanish:

$$\begin{aligned} F_{mlm'l'} &= 2\delta_{m,m'}\delta_{l,l'} \text{ Classical Parton Cascade ,} \\ F_{mlm'l'} &= \delta_{m,n_s}\delta_{m',n_s} \text{ Coherent Factorization .} \end{aligned} \tag{38}$$

Simple analytic expressions can be obtained for the form factors if the ensemble average over the interaction times is taken as in eq. (20). The form factors involve a sum of four terms of the form

$$\begin{aligned} \left\langle\, e^{i\sum_{j=1}^{n_s}(t_j - t_0)\omega_j} \,\right\rangle &= \left\langle\, e^{i\sum_{j=1}^{n_s}\tau_j\tilde{\omega}_j} \,\right\rangle = \prod_{j=1}^{n_s}\int_0^\infty \frac{d\tau_j}{\lambda_j} e^{-\frac{\tau_j}{\lambda_j}(1 - i\lambda_j\tilde{\omega}_j)} \\ &= \prod_{j=1}^{n_s}\frac{1}{1 - i\lambda_j(\omega_j + \cdots + \omega_{n_s})} \,, \end{aligned} \tag{39}$$

where $\tau_j \equiv t_j - t_{j-1}$, $\tilde{\omega}_j = \omega_j + \cdots + \omega_{n_s}$. Here $\lambda_j = \langle \tau_j \rangle$ is the average distance between the $j-1$ and j^{th} scattering centers. This ensemble is characterized by the following distribution of $t = t_k - t_0$:

$$\begin{aligned} P_k(t) &= \langle\, \delta(t_k - t_0 - t) \,\rangle = \int \frac{d\omega}{2\pi} e^{-i\omega(t_k - t_0)} \prod_{j=1}^{k}\frac{1}{1 - i\omega\lambda_j} \\ &= \sum_{j=1}^{n_s}\frac{e^{-t/\lambda_j}}{\lambda_j}\left(\prod_{l\neq j}^{k}\frac{1}{(1 - \lambda_l/\lambda_j)}\right) \quad \stackrel{\lambda_k = \lambda}{\longrightarrow} \quad \frac{e^{-t/\lambda}}{\lambda}\frac{(t/\lambda)^{k-1}}{(k-1)!} \,. \end{aligned} \tag{40}$$

The geometry of the plasma is particularly simple if $\lambda_k = \lambda$, with

$$\langle\, (t_k - t_0) \,\rangle = k\lambda \,, \qquad \langle\, (t_j - t_0)(t_k - t_0) \,\rangle = k(j+1)\lambda^2 \,, \;\; j \geq k \,.$$

For more realistic ensembles corresponding to an expanding target with centers distributed according to $\rho(z,t)$. The form factors must be evaluated numerically via

$$\begin{aligned} \left\langle\, e^{i\sum_{j=1}^{n_s}(t_j - t_0)\omega_j} \,\right\rangle &= \frac{1}{P_n}\int_{t_0}^{\infty} dt_n e^{-\chi(\infty, t_n)} \int_{t_0}^{t_n} dt_{n-1} \cdots \int_{t_0}^{t_2} dt_1 \\ &\quad \times \left(\, \prod_k \sigma_{el}\, \rho(z_k = t_k, t_k)\, e^{i(t_j - t_0)\omega_j}\, e^{-\chi(t_k, t_{k-1})} \right) \,, \\ \chi(t, t') &= \int_{t'}^{t} d\,\hat{t}\; \sigma_{el}\rho(z = \hat{t}, \hat{t}\,) \,, \\ P_{n_s} &= e^{-\chi(\infty, t_0)}\frac{\chi^{n_s}(\infty, t_0)}{n_s!} \,. \end{aligned} \tag{41}$$

Here $\chi(t, t')$ is the average number of interactions a jet moving with the speed of light through the expanding target suffers between t' and t with σ_{el} given by eq. (22). Note

that P_{n_s} is the probability that only n_s out of a large possible $N \gg 1$ target interactions occur in the medium. In this more general case, the interactions are distributed as

$$\begin{aligned} P_k(t_k) &= P_{n_s} \frac{d\gamma(t_k)}{dt_k} (1-\gamma(t_k))^{n_s-k} \gamma^{k-1}(t_k) \; , \\ \gamma(t) &= \chi(t,t_0)/\chi(\infty,t_0) \; . \end{aligned} \tag{42}$$

For a static uniform slab of thickness L with density $\rho_0 \theta(L-z)$

$$\left\langle \; e^{i\sum_{j=1}^{n_s} t_j \omega_j} \; \right\rangle = \frac{n_s!}{L^{n_s}} \int_0^L dt_{n_s} e^{i t_{n_s} \omega_{n_s}} \cdots \int_0^{t_2} dt_1 e^{i t_1 \omega_1} \; , \tag{43}$$

It is instructive to compare eq. (43) with eq. (39). In the slab geometry setting $t_0 = 0$

$$\langle \, t_k \, \rangle = \frac{k \; L}{(n_s+1)} \; , \qquad \langle \, t_j t_k \, \rangle = \frac{k(j+1) \; L^2}{(n_s+2)(n_s+1)} \; , \;\; j \geq k \; .$$

Thus, if we set $\lambda \equiv L/(n_s+1)$

$$\langle \, t_k \, \rangle = k\lambda \; , \qquad \langle \, t_j t_k \, \rangle = k(j+1)\lambda^2 \frac{(n_s+1)}{(n_s+2)} \; , \;\; j \geq k \; .$$

For $n_s \gg 1$ the geometry of both ensembles is quite similar if set λ appropriately. Near the factorization limit, where $\sum_{j=1}^{n_s} \lambda \omega_j \ll 1$ we can expand

$$\left\langle \; e^{i\sum_{j=1}^{n_s} (t_j - t_0)\omega_j} \; \right\rangle \approx 1 + i\lambda \sum_{j=1}^{n_s} j\omega_j - r \; \lambda^2 \sum_{j=i}^{n_s} \sum_{k=1}^{j} k(j+1) \omega_j \omega_k \; , \tag{44}$$

where the only difference between eq. (39) and eq. (43) is that $r = 1$ in the first case and $r = (n+1)/(n+2)$ in the second case. The deviations from factorization can therefore be reasonably well approximated by our simpler ensemble. On the other hand, for large $\lambda\omega_j$, the slab form factors oscillate due to the sharp boundary while the form factors in the eq. (39) ensemble decrease monotonically. The deviations from the classical parton cascade limit is therefore more sensitive to the detailed form of the geometry of the medium. We will continue to use below eq. (39) to reduce the complexity of the calculation.

Since the final pattern of jet quenching depends on the actual distributions and correlations among scattering centers in general, one should evaluate eq. (36) numerically for any actual application to nucleus-nucleus collisions [12].

3.5 Relative Conditional Probabilities

It is tempting to identify as in eqs. (15,16)

$$R_g^{(n_s)}(\vec{k}) = \frac{1}{16\pi^3} \frac{\rho_{rad}^{(n_s)}(\vec{k},\vec{p})}{\rho_{el}^{(n_s)}(\vec{p}+\vec{k})} \tag{45}$$

as the invariant soft gluon number distribution associated with n_s interactions. However, because the radiated gluon can rescatter in addition to the incident jet, the conditional double inclusive density, $\rho_{rad}^{(n_s)}$, cannot be factored into a product of the elastic distribution and the gluon number distribution as in the case of QED. The problem is that the production and gluon rescattering amplitudes interfere, and $\rho_{rad}^{(n_s)}$ includes the process where the gluon is radiated before the first collision and the n_s recoil target partons are produced by elastic scattering with the produced gluon rather than the incident jet. Therefore, we interpret $R_g^{(n_s)}$ as a relative conditional probability density to find a gluon in the final state with momentum k given a final observed jet with momentum p and given that n_s target recoil partons are observed (with any momentum).

Let P_{n_s} be the *a priori* probability that there are n_s scattering centers or target recoil partons. The final jet quenched spectrum is then given by

$$\rho_J(\vec{p}) = \sum_{n_s} \frac{P_{n_s}}{Z_{n_s}} \left(\rho^{(0)}(\vec{p}) + \int \frac{d^3\vec{k}}{\omega}\, \rho^{(0)}(\vec{p}+\vec{k})\; R_g^{(n_s)}(\vec{k}\,) \right) \;, \tag{46}$$

where $\rho^{(0)}(p)$ is the initial hard jet distribution in eq. (12), and where the (wavefunction) renormalization factor

$$Z_{n_s} = 1 + \int \frac{d^3\vec{k}}{\omega} R_g^{(n_s)}(\vec{k}\,) \tag{47}$$

insures that the integrated total number of jets is conserved. It in fact corresponds to the first order in α_s term in the expansion of the inverse Sudakov factor for the probability that no radiation accompanies the jet. In this paper we only compute, $R_g^{(n_s)}(\vec{k}\,)$, which limits the discussion to single gluon emission: $R_g^{(n_s)}(\vec{k}\,) \equiv R_g^{(n_s,n_g=1)}(\vec{k}\,)$.

Unfortunately, even in the $n_s = 0$ case the single gluon approximation is not accurate because

$$Z_0 = 1 + \frac{C_R\alpha_s}{\pi} \log^2(E_0/\mu) \;, \tag{48}$$

can be significantly bigger than one, indicating that multigluon emission from the hard vertex is necessary. Summing the double logarithms leads to a modified Bessel function multiplicity distributions as discussed in [19]. The DLA leads to [19],

$$\begin{aligned} Z_0 &= 1/I_0(r(E)) \;, \\ r(E) &= \sqrt{8C_R\alpha/\pi}\log(E/\mu) \;, \\ \langle n_g \rangle &= \frac{r}{2}\frac{I_1(r)}{I_0(r)} \approx \frac{r(E)}{2} \quad . \end{aligned} \tag{49}$$

In the general case of multiple gluon emission, as required in practical applications, we must generalize eqs. (46,47) as

$$\rho_J(\vec{p}) = \sum_{n_s} \frac{P_{n_s}}{Z_{n_s}} \left(\rho^{(0)}(\vec{p}) + \sum_{n_g=1}^{\infty} \int \prod_{i=1}^{n_g} \frac{d^3\vec{k}_i}{\omega_i}\, \rho^{(0)}(\vec{p}+\sum_j \vec{k}_j\,) R_g^{(n_s,n_g)}(\vec{k}_1,\cdots,\vec{k}_{n_g}\,) \right) \;, \tag{50}$$

where the (wavefunction) renormalization factor becomes

$$Z_{n_s} = 1 + \sum_{n_g=1}^{\infty} \int \prod_{i=1}^{n_g} \frac{d^3\vec{k}_i}{\omega_i} \, R_g^{(n_s,n_g)}(\vec{k}_1, \cdots, \vec{k}_{n_g}) \, . \tag{51}$$

The implementation of this approach requires Monte–Carlo methods that will be discussed in the subsequent paper [12].

From the above formulas, we can infer that the exclusive n_g gluon number distributions associated with n_s scattering is

$$\omega_1 \cdots \omega_{n_g} \frac{dN_g^{(n_s,n_g)}}{d^3\vec{k}_1 \cdots d^3\vec{k}_{n_g}} = \frac{1}{Z_{n_s}} R_g^{(n_s,n_g)}(\vec{k}_1, \cdots, \vec{k}_{n_g}) \, . \tag{52}$$

4 Case of One Scattering Center

We consider in this section the simplest case of gluon radiation in hard processes followed by one rescattering.

4.1 Reduced Amplitudes and Transverse Profile Dependence

The three graphs that generalize the Gunion-Bertsch analysis [6] to this case are shown in Fig. 3.

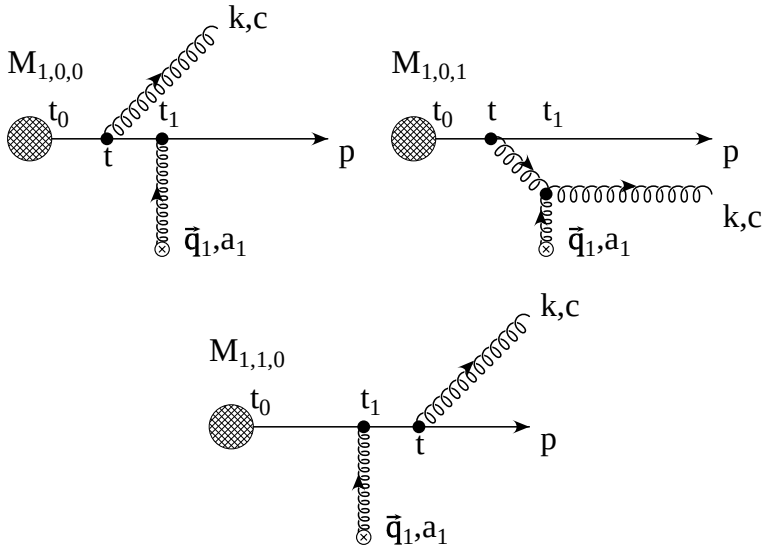

Fig. 3. Three contributions to the soft gluon radiation amplitude $M_J \otimes M_1$ in case of one scattering.

Following BDMPS [9], the three radiative amplitudes are given by

$$\mathcal{M}_{1,0,0} \;=\; 2ig_s \frac{\vec{\epsilon}_\perp \cdot \vec{k}_\perp}{k_\perp^2} (e^{it_1 \frac{k_\perp^2}{2\omega}} - e^{it_0 \frac{k_\perp^2}{2\omega}}) a_1 c \, , \tag{53}$$

$$\mathcal{M}_{1,0,1} = 2ig_s \frac{\vec{\epsilon}_\perp \cdot (\vec{k}-\vec{q}_1)_\perp}{(k-q_1)_\perp^2} e^{it_1 \frac{k_\perp^2-(k-q_1)_\perp^2}{2\omega}} \times$$
$$\times (e^{it_1 \frac{(k-q_1)_\perp^2}{2\omega}} - e^{it_0 \frac{(k-q_1)_\perp^2}{2\omega}}) \, [c, a_1] \ , \tag{54}$$
$$\mathcal{M}_{1,1,0} = 2ig_s \frac{\vec{\epsilon}_\perp \cdot \vec{k}_\perp}{k_\perp^2} (-e^{it_1 \frac{k_\perp^2}{2\omega}}) c a_1 \ . \tag{55}$$

Here t_1 is the impulse time when $\vec{q}_{1\perp}$ transverse momentum is imparted to the jet relative to its axis $\vec{p}$. The color charge flow is modified by an additional matrix a_1, that appears in different orderings relative to the radiation vertex c in these amplitudes. A new infrared singularity $\vec{k}_\perp - \vec{q}_{1\perp} = 0$ emerges due to the dipole radiation associated with the exchanged gluon. However, the phase factors cancel at that point and the amplitude remains finite proportional to $t_1 - t_0$.

To keep the somewhat cumbersome notation compact we introduce the following reduced amplitudes

$$\vec{H} = \frac{\vec{k}_\perp}{k_\perp^2} \ , \qquad \vec{C}_{(i_1 i_2 \cdots i_m)} = \frac{(\vec{k} - \vec{q}_{i_1} - \vec{q}_{i_2} - \cdots - \vec{q}_{i_m})_\perp}{(k - q_{i_1} - q_{i_2} - \cdots - q_{i_m})_\perp^2} \ ,$$
$$\vec{B}_i \equiv \vec{H} - \vec{C}_i \ , \qquad \vec{B}_{(i_1 i_2 \cdots i_m)(j_1 j_2 \cdots i_n)} \equiv \vec{C}_{(i_1 i_2 \cdots j_m)} - \vec{C}_{(j_1 j_2 \cdots j_n)} \ ,$$

which we call "hard", "cascade", "Gunion–Bertsch", and "Gunion–Bertsch cascade". The time integrals involve energy differences

$$\omega_0 = k_\perp^2/2\omega = 1/t_f \ , \quad \omega_{(i_1 i_2 \cdots i_m)} = (k - \vec{q}_{i_1} - \vec{q}_{i_2} - \cdots - \vec{q}_{i_m})_\perp^2/2\omega \ ,$$
$$\omega_{0i} \equiv \omega_0 - \omega_i \ , \quad \omega_{(i_1 i_2 \cdots i_m)(j_1 j_2 \cdots i_n)} \equiv \omega_{(i_1 i_2 \cdots i_m)} - \omega_{(j_1 j_2 \cdots i_n)} \ ,$$

that control the formation physics. A quantity with two indices is defined to be the difference of two quantities with a single index (note that an array in parentheses counts as a single index). Thus, for example $t_{10} \equiv t_1 - t_0$, $\omega_{10} \equiv \omega_1 - \omega_0$.

To make contact with the Gunion-Bertsch bremsstrahlung radiation distribution [6] and facilitate the physics interpretation we rearrange the sum of the three amplitudes as follows:

$$\mathcal{M}_1 = -2ig_s e^{it_0\omega_0} \vec{\epsilon}_\perp \cdot \left\{ \vec{H} a_1 c + \vec{B}_1 e^{it_{10}\omega_0} \, [c, a_1] + \vec{C}_1 e^{-it_{10}(\omega_1 - \omega_0))} \, [c, a_1] \right\} . \tag{56}$$

Including an adiabatic damping factor $e^{-\epsilon t_1}$, we see that for $t_1 \to \infty$ the pure hard radiation formula for the $n_s = 0$ case is recovered.

$$\lim_{t_1 \to +\infty} \mathcal{M}_1 = a_1 \, \mathcal{M}_0 \ . \tag{57}$$

On the other hand, in the $t_0 \to -\infty$ limit,

$$\mathcal{M}_1 \to -2ig_s \vec{\epsilon}_\perp \cdot \vec{B}_1 e^{it_1\omega_0} \, [c, a_1] = \mathcal{M}_{GB} \ , \tag{58}$$

corresponding to the isolated bremsstrahlung amplitude. This leads to the characteristic GB radiation spectrum

$$\frac{dN_g^{(GB)}}{dyd^2\vec{k}_\perp} = C_A \frac{\alpha_s}{\pi^2} \frac{q_1^2}{k_\perp^2 (k-q_1)_\perp^2} \, , \tag{59}$$

that has **to be averaged** over the transfered momentum. Here only the adjoint Casimir $C_A = N_c$ enters and the result is independent of C_R. Note that in this limit, the $\vec{k}_\perp = \vec{q}_{1\perp}$ is exposed and in [6] is regulated with an appropriate hadronic form factor.

For the theoretical application to a parton penetrating through infinite matter, this singularity is regulated by the in-medium self energy of the gluon, $\Pi^{\mu\nu}(k)$. The transverse plasmon modes satisfy $\omega^2 = k^2 + \Pi_T(\omega, k)$ in an infinite plasma medium, with $\Pi_T(\omega_{pl}(k), k) \approx \omega_{pl}^2 \approx \mu^2/3$ and $\mu^2 = g^2 T^2 (2N_c + N_f)/6$ is the Debye screening mass in thermal pQCD. For $k_z \gg T$ on the other hand, $\omega_{pl}(k) \approx k_z + (k_\perp^2 + \mu^2/2)/(2k_z)$. Thus the infrared singularities are regulated by a scale $\sim \mu^2$. Near the light cone, the one loop approximation for the self energy is not likely to remain accurate though. In fact, gauge invariance requires that the same μ^2 screening scale regulate both the potential singularity and the above infrared divergences [8, 9].

In contrast to the above, $t_0 \to -\infty$ limit, the $\vec{k}_\perp = \vec{q}_{1\perp}$ singularity is also regulated by canceling phases for t_{10} finite. In this case of interest here, it is the maximum of μ^2 and ω/t_{10} that regulates that singularity. For large $\omega \gg \omega_{BH} = \mu^2\lambda/2$, most important for energy loss, the latter scale in fact sets the characteristic transverse momentum of the gluon in the $k_\perp > \mu$ domain.

Summing over final polarizations and colors and averaging over initial colors, the $n_s = 1$ gluon distribution from eqs. (28,53-55) is

$$\begin{aligned} \rho_{rad}^{(1)}(k,p) &\approx |J(p+k)|^2 \int \frac{d^2\vec{q}_1}{(2\pi)^2} \frac{d^2\vec{q}_1'}{(2\pi)^2} V(\vec{q}_1) V^*(\vec{q}_1') \frac{C_2(i)}{D_A} T(\vec{q}_{1\perp} - \vec{q}_{1\perp}') \\ &\times \left\langle \, \mathrm{Tr} \left(\sum_{1,m,l,m',l'} \mathcal{M}_{1,m,l}(k,p;\vec{q}_{1\perp}) \mathcal{M}^\dagger_{1,m',l'}(k,p;\vec{q}_{1\perp}') \right) \right\rangle_t . \end{aligned} \tag{60}$$

The main complexity in the above expression arises from the mixing of different $\vec{q}_1$ and $\vec{q}_1'$ components. However, if the transverse profile $T(\vec{x}_\perp)$ of the target is approximately a constant over dimensions $R \gg 1/\mu$, then the difference $|\vec{q}_1 - \vec{q}_1'| \sim 1/R$ can be neglected in *some* of the terms. The only sensitive dependence of that difference arises through the phase factors in eq. (53-55). A systematic expansion in that difference is possible changing variables to $\vec{Q} = (\vec{q}_1 + \vec{q}_1')/2$ and $\vec{q} = \vec{q}_1 - \vec{q}_1'$ and expanding in $\vec{q}$. To leading order in this expansion

$$\rho_{rad}^{(1)}(k,p) = 4g_s^2 \, |J(p+k)|^2 \int \frac{d^2\vec{Q}}{(2\pi)^2} \frac{C_2(i)}{D_A} |V(\vec{Q})|^2 \int \frac{d^2\vec{q}}{(2\pi)^2} \, T(\vec{q}) \times$$

$$
\begin{aligned}
&\Big\langle \mathrm{Tr}\,\Big((\vec{H}a_1c+\vec{B}_Qe^{it_{10}\omega_0}\,[c,a_1])\cdot(\vec{H}ca_1+\vec{B}_Qe^{-it_{10}\omega_0}\,[a_1,c])\Big)\\
&+\mathrm{Tr}\,\Big(|\vec{C}_Q|^2e^{-it_{10}(\omega_1-\omega_1')}\,[c,a_1]\,[a_1,c]\Big)\\
&+\mathrm{Tr}\,\Big((\vec{H}a_1c+\vec{B}_Qe^{it_{10}\omega_0}\,[c,a_1])\cdot\vec{C}_Qe^{+it_{10}(\omega_1-\omega_0)}\,[a_1,c]\Big)\\
&+\mathrm{Tr}\,\Big((\vec{H}a_1c+\vec{B}_Qe^{-it_{10}\omega_0}\,[c,a_1])\cdot\vec{C}_Qe^{-it_{10}(\omega_1'-\omega_0)}\,[a_1,c]\Big)\Big\rangle_{t_1}\quad .
\end{aligned}
\tag{61}
$$

Note that $\omega_1=(\vec{k}-\vec{Q}-\vec{q}/2)^2/2\omega,\ \omega_1'=(\vec{k}-\vec{Q}+\vec{q}/2)^2/2\omega$, and therefore, the extra phase factor multiplying the diagonal cascade contribution has a phase

$$\vec{b}_1\cdot\vec{q}=t_{10}(\vec{k}-\vec{Q})\cdot\vec{q}/\omega\ ,$$

where we drop $\mathcal{O}(t_{10}\mu^2/\omega)$ terms. The integration over $d^2\vec{q}$ transforms $T(\vec{q}\,)$ therefore into transverse spatial profile $T(\vec{b}_1)$ evaluated at the impact parameter

$$\vec{b}_1=t_{10}(\vec{k}-\vec{Q})/\omega\ ,$$

at which a gluon produced at the origin with transverse momentum $\vec{k}-\vec{Q}$ would pass by the scattering center at $z_1=ct_1$. This tends to suppress the cascade contribution as intuitively expected for kinematic configurations where the gluon "misses" the target. On the other hand, the diagonal hard and Gunion-Bertsch contributions remain unsuppressed since the rescattering of the jet occurs at zero impact parameter in the high energy limit. For a broad target, the transverse profile is approximately a constant $T(\vec{b}_1)\approx T(0)\sim 1/\pi R^2$. However, in general the cascade term is modulated by a relative target transverse profile factor

$$\mathcal{T}(\vec{b}_1)\equiv T(\vec{b}_1)/T(0)\ .$$

The relative conditional probability for gluon radiation in this $n_s=1$ case for a fixed momentum transfer $\vec{Q}_\perp\to\vec{q}_{1\perp}$ therefore reduces to

$$
\begin{aligned}
R_g^{(1)}(\vec{k},\vec{q}_{1\perp}) \;=\;& C_R\frac{\alpha_s}{\pi^2}\Big\{\vec{H}^2+R\,(\vec{B}_1^{\,2}+\mathcal{T}(\vec{b}_1)\,\vec{C}_1^{\,2})-R\,\Big(\vec{H}\cdot\vec{B}_1\cos(t_{10}\omega_0)\Big)\\
&-R\,\mathcal{T}(\vec{b}_1/2)\,\Big(\vec{H}\cdot\vec{C}_1\cos(t_{10}\omega_{10})-2\vec{C}_1\cdot\vec{B}_1\cos(t_{10}\omega_1)\Big)\Big\}\quad .
\end{aligned}
\tag{62}
$$

Note that the transverse profile factor modulates the interference term between $\vec{C}$ and $\vec{H}+\vec{B}$ at the average impact parameter, $\vec{b}_1/2$ of the jet and gluon at the scattering center. Note that for $t_{10}\to 0$ there is a perfect cancellation of all but the hard radiation term since $b_1\propto t_{10}\to 0$ and $\mathcal{T}(b=0)=1$. In fact, this factorization limit is recovered more generally when $t_{10}/\omega\to 0$.

The first three terms corresponds to the diagonal terms which are independent of the time between the hard production point and the rescattering point. The next three terms are oscillating interference terms. The color factor $R=C_A/C_R$ is 1 for a gluon jet and 9/4 for a quark jet.

It is interesting to note that if the momentum transfer $\vec{q}_1$ in the scattering vanishes, then $\vec{B}_1=0$, $\vec{C}=\vec{H}$, and $\omega_1=\omega_0$ and the above distribution reduces to the zero

scattering case in the previous section. This is a manifestation of gauge invariance requiring a finite $\vec{q}_1$ to generate a color dipole that can modify the hard radiation pattern.

It is clear that the classical incoherent parton cascade limit corresponds to assuming that all the oscillating interference term average to zero. In that case, the final gluon distribution is a sum of the initial hard radiation plus an isolated Gunion-Bertsch bremsstrahlung plus a rescattering "cascade" contribution reflecting the modification of the final transverse momentum spectrum due to rescattering of a gluon produced at t_0. That latter term broadens the transverse distribution of the emitted gluons.

4.2 Relative Conditional Probability for $n_s = 1$

The magnitude of the interference effects in eq. (62) is controlled by dimensionless variables

$$\kappa \equiv \frac{\vec{k}_\perp^{\,2}}{\mu^2} \, , \quad \xi \equiv \frac{\lambda\mu^2}{2\omega} = \frac{\omega_{BH}}{\omega} \, , \quad \kappa_1 \equiv \frac{(\vec{k}-\vec{q}_1)_\perp^2}{\mu^2} \, , \quad \theta_1 \equiv \frac{\vec{q}_{1\perp}^{\,2}}{\mu^2} \, . \tag{63}$$

Note that this averaged interference cosine is small when $\xi\kappa_i > 1$. This is the kinematic region where the relevant formation time, $\tau_i = 1/\omega_i = 2\omega/(\vec{k}_\perp - \vec{q}_{i\perp})^2$, is smaller than the mean free path. For a fixed energy ω this restricts the angle of induced emission radiation to exceed $\theta_{min} = 1/\sqrt{(\omega\lambda)}$. Below θ_{min} complete destructive interference cancels all but the hard production amplitude.

The time averaged relative conditional distribution for fixed $\vec{q}_{1\perp}$ can be written as

$$R_g^{(1)}(\vec{k},\vec{q}_{1\perp}) \;\; = \;\; R_g^{(0)}(\vec{k})\mathcal{F}^{(1)}(\vec{k}_\perp,\vec{q}_{1\perp},\xi) \, , \tag{64}$$

where $R_g^{(0)}$ is given by eq. (15) and the modification factor due to $n_s = 1$ rescattering is given by

$$\begin{aligned}
\mathcal{F}^{(1)} \;\; &= \;\; \frac{\kappa^2}{\tilde{\kappa}^2} + R\left(\frac{\kappa^2}{\tilde{\kappa}^2} + 2\frac{\kappa\kappa_1}{\tilde{\kappa}_1^2} - 2\frac{\kappa\Delta\kappa}{\tilde{\kappa}\tilde{\kappa}_1}\right) - R\left(\frac{\kappa^2}{\tilde{\kappa}^2} - \frac{\kappa\Delta\kappa}{\tilde{\kappa}\tilde{\kappa}_1}\right)\frac{1}{1+\xi^2\tilde{\kappa}^2} \\
&\quad -R\left(\frac{\kappa\Delta\kappa}{\tilde{\kappa}\tilde{\kappa}_1}\right)\frac{1}{1+\xi^2(\tilde{\kappa}-\tilde{\kappa}_1)^2} + 2R\left(\frac{\kappa\Delta\kappa}{\tilde{\kappa}\tilde{\kappa}_1} - \frac{\kappa\kappa_1}{\tilde{\kappa}_1^2}\right)\frac{1}{1+\xi^2\tilde{\kappa}_1^2} \\
&= \;\; \frac{\kappa^2}{\tilde{\kappa}^2} + R\,\xi^2\left\{\frac{\kappa^2}{1+\xi^2\tilde{\kappa}^2} + 2\frac{\kappa\kappa_1}{1+\xi^2\tilde{\kappa}_1^2}\right. \\
&\quad \left. -\left(\frac{\kappa\Delta\kappa}{\tilde{\kappa}\tilde{\kappa}_1}\right)\left(\frac{2\tilde{\kappa}_1^2}{1+\xi^2\tilde{\kappa}_1^2} - \frac{(\tilde{\kappa}-\tilde{\kappa}_1)^2}{1+\xi^2(\tilde{\kappa}-\tilde{\kappa}_1)^2} + \frac{\tilde{\kappa}^2}{1+\xi^2\tilde{\kappa}^2}\right)\right\} \, ,
\end{aligned} \tag{65}$$

where $\Delta\kappa = \kappa - \vec{k}_\perp\cdot\vec{q}_{1\perp}/\mu^2 = (\kappa^2+\kappa_1^2-\theta_1^2)/2$. The tilde denotes $\tilde{\kappa}_i \equiv \kappa_i + \epsilon^2$, that results when a plasmon mass shift, $\omega_{pl}^2 = \epsilon^2\mu^2$, is introduced in all propagators.

Eq. (65) shows that for finite ξ, the $\vec{k}_\perp = \vec{q}_{1\perp}$ singularity of free space perturbation theory eq. (59) is automatically regulated by the interference terms. For finite ξ

therefore we can safely take the $\epsilon = 0$ limit and write

$$\mathcal{F}^{(1)} = 1 + R\,\xi^2 \left\{ \frac{\kappa^2}{1+\xi^2\kappa^2} + 2\frac{\kappa\kappa_1}{1+\xi^2\kappa_1^2} - \left(\frac{\Delta\kappa}{\kappa_1}\right)\left(\frac{2\kappa_1^2}{1+\xi^2\kappa_1^2} - \frac{(\kappa-\kappa_1)^2}{1+\xi^2(\kappa-\kappa_1)^2} + \frac{\kappa^2}{1+\xi^2\kappa^2}\right)\right\} . \quad (66)$$

However, in the *formal* classical parton cascade limit with $\xi \to \infty$ ($\omega \gg \omega_{BH}$) the apparent singularity is exposed unless $\epsilon \neq 0$:

$$\mathcal{F}^{(1)}(\vec{k}_\perp, \vec{q}_{1\perp}, \xi = \infty) = \frac{\kappa^2}{\tilde{\kappa}^2}(1+R) + 2R\frac{\kappa}{\tilde{\kappa}_1}\left(\frac{\kappa_1}{\tilde{\kappa}_1} - \frac{\Delta\kappa}{\tilde{\kappa}}\right) \stackrel{\epsilon\to 0}{\longrightarrow} \left(\vec{H}^{\,2} + R\left(\vec{B}_1^2 + \vec{C}_1^2\right)\right)/\vec{H}^2 . \quad (67)$$

To compare the full quantum parton cascade modification factor eq. (66) to the incoherent classical parton cascade result, we regulated the singular classical limit with $\epsilon = 1$

$$\mathcal{F}_{cl}^{(1)}(\vec{k}_\perp, \vec{q}_{1\perp}) \equiv \mathcal{F}_{cl}^{(1)}(\vec{k}_\perp, \vec{q}_{1\perp}, \infty)\Big|_{\epsilon=1} . \quad (68)$$

In the opposite $\xi \to 0$ limit, on the other hand, we see that the factorization theorem, $\mathcal{F}^{(1)} \to 1$, is recovered.

Another interesting limit is $k_\perp \gg q_{1\perp} \sim \mu$. In that kinematic range, the induced GB bremsstrahlung can be ignored, ($\vec{B}_1^2 \approx 0$) but the cascade term survives ($\vec{C}_1^2 \to \vec{H}^2$). Therefore, in the $\mu \ll k_\perp < \omega$ kinematic regime

$$\mathcal{F}^{(1)}(\vec{k}_\perp, \vec{q}_{1\perp}) \stackrel{\vec{k}_\perp^{\,2} \gg \mu^2}{\longrightarrow} 1 + R . \quad (69)$$

This enhancement of the high $k_\perp$ tail arises because rescattering of the gluon is enhanced by a color factor $R = C_A/C_R$ relative to the jet. As we shall see, this is a special case of the general asymptotic $k_\perp^2 \gg n_s\mu^2$ form in the case of n_s collisions:

$$\mathcal{F}^{(n_s)}(\vec{k}_\perp, \vec{q}_{1\perp}, \cdots \vec{q}_{n_s\perp}) \stackrel{\vec{k}_\perp^{\,2} \gg n_s\mu^2}{\longrightarrow} (1+R)^{n_s} . \quad (70)$$

Although it is possible to integrate over the momentum transfers analytically, the result even in the case of one scattering center is not instructive. Therefore, we average $\mathcal{F}^{(1)}$ over $\vec{q}_{1\perp}$ numerically for different values of $\xi = \omega_{BH}/\omega$:

$$F^{(1)}(\kappa, \xi) = \langle\, \mathcal{F}^{(1)} \,\rangle = \int_0^{s/4\mu^2} \frac{d\theta_1}{(\theta_1+1)^2} \int_0^{2\pi} \frac{d\phi_1}{2\pi}\, \mathcal{F}^{(1)}(\kappa, \theta_1, \phi_1, \xi) . \quad (71)$$

Note that we keep the large $s/4\mu^2 \approx 6E_{jet}T/4\mu^2$ upper bound in the integration finite because the kinematic boundaries include regimes where $E^2 \geq \omega^2 \geq k_\perp^2 \geq s$.

In Fig. 4a the three components of the classical parton cascade envelop ($\xi = \infty$) for an initial quark jet are shown for the case $\mu = 0.5$ GeV as a function of the logarithmic "angle" $\log_{10}(\kappa)$. The Hard factorization term corresponds to the unit curve. The GB induced radiation component dominates at small κ and the cascade contribution is only

important at large κ. The bump at $\kappa \sim 5$ is the remnant of the logarithmic singularity exposed in the $\xi = \infty$ limit, but regulated here with a plasmon mass $\omega_{pl} = \mu = 0.5$ GeV.

Fig. 4b shows the ensemble averaged quantum modification factor, $F^{(1)}$, with $\mu = 0.5$ GeV, $\lambda = 1$ fm/c ($\omega_{BH} \approx 0.63$ GeV) for seven different gluon energies ω. These correspond to $\xi = 0.013,\ 0.031,\ 0.063,\ 0.13,\ 0.31,\ 0.63$, and 1.3 that cover an energy range 0.5 GeV $< \omega <$ 50 GeV . In each case, the curves are cut off at the kinematic bound

$$\kappa_{max} = \frac{\omega^2}{\mu^2} = \frac{(\lambda\mu)^2}{4\xi^2} \ ,$$

which corresponds to right angle radiation relative to the jet axis. Here $(\lambda\mu)^2/4 \approx 1.5$. The curves illustrate well how the total destructive interference (LPM effect) for $\kappa\xi < 1$ reduces $F^{(1)}$ to unity. In particular, the induced Gunion-Bertsch radiation component in Fig. 4a is almost completely suppressed due to interference with the hard production amplitude. Only the cascade term modifies the spectrum considerably at large $k_\perp$. The onset of significant medium modification can be seen to follow qualitatively the point $\kappa_c = 1/\xi$.

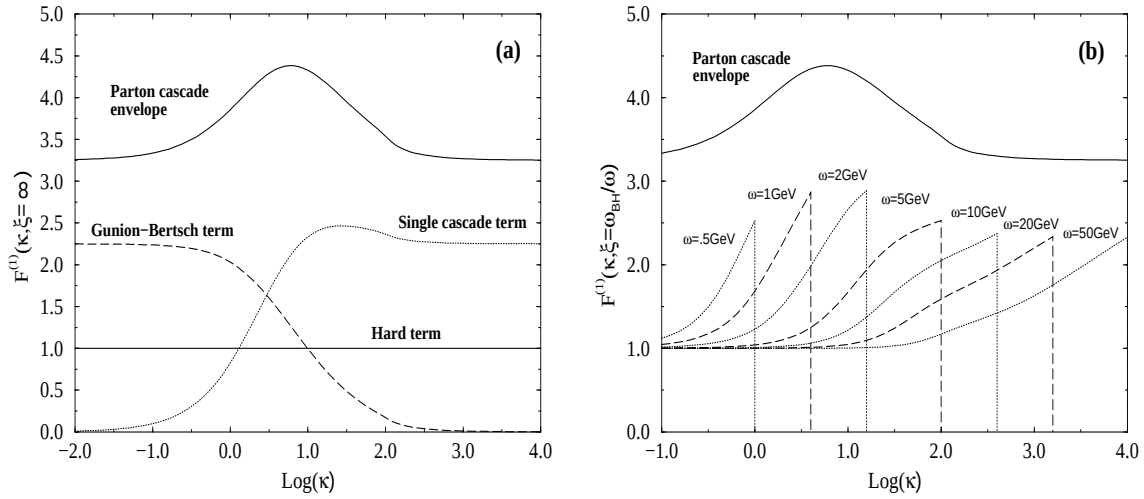

Fig. 4. (a) The normalized time-independent envelopes and separate contributions to the conditional probability distribution of gluons associated with a single rescattering $n_s = 1$ of quark jet ($E_{jet} = 50$GeV) is shown as a function of the logarithmic "angle", $\log_{10} k_\perp^2/\mu^2$ with $\mu = 0.5$ GeV. These curves correspond to the incoherent parton cascade limit. (b) For finite $t_{10} = 1$ fm/c case destructive interference limits the corrections to the hard self-quenched distribution to higher angles as shown for different gluon energies.

It is convenient to define in general the reduced modification factor $f^{(n_s)}(\kappa, \xi)$ through

$$F^{(n_s)}(\kappa, \xi) \equiv \left\{1 + ((1+R)^{n_s} - 1)\ f^{(n_s)}(\kappa, \xi)\right\}\ \theta\left(\frac{(\lambda\mu)^2}{4\xi^2} - \kappa\right) \ , \qquad (72)$$

which isolates the kinematic boundary and the asymptotic color scaling factor. Note that the incoherent classical parton cascade envelope is not reached for any reasonable values of $\lambda\mu$ due the finite kinematic boundaries.

5 Case of Two Scattering Centers

The relative conditional probability $R_g^{(2)}(\vec{k}\,)$ can be obtained through the averaging of the square of the matrix element $\mathcal{M}_2$ on the scattering potentials in the $\vec{q}_1$ and $\vec{q}_2$ space.

In Appendix A we listed the matrix elements connected to the seven planar diagrams, contributing to the soft gluon radiation. The sum of the matrix elements can be written as

$$\begin{aligned}\mathcal{M}_2 &= -2ig_s e^{it_0\omega_0}\times\vec{\epsilon}_\perp\cdot\Big\{\vec{H}a_2a_1c+\vec{B}_1e^{it_{10}\omega_0}a_2\,[c,a_1]\\ &+\vec{B}_2e^{it_{20}\omega_0}\,[c,a_2]\,a_1+\vec{B}_{2(12)}e^{i(t_{20}\omega_0-t_{21}\omega_2)}\,[[c,a_2],a_1]\\ &+\vec{C}_1e^{-it_{10}\omega_{10}}a_2\,[c,a_1]+\vec{C}_2e^{-it_{20}\omega_{20}}a_1\,[c,a_2]\\ &+\vec{C}_{(12)}e^{i(t_{20}\omega_0-t_{21}\omega_2-t_{10}\omega_{(12)})}\,[[c,a_2],a_1]\Big\}\ . \end{aligned}\tag{73}$$

In the limit where all $t_i-t_j=0,\ t_i>t_j,\ i,j=1,2$ one can easily see that all the terms but the "hard" scattering cancel

$$\mathcal{M}_2 = -2ig_se^{it_0\omega_0}\,\vec{\epsilon}_\perp\cdot\vec{H}a_2a_1c\,.\tag{74}$$

The GB $t_0\to-\infty$ limit and the connection to the BDMPS [9] result we discuss in Appendix B.

After calculating the appropriate color factors in eqs. (92)-(93) we obtain

$$\begin{aligned}\mathrm{Tr}\left(\mathcal{M}_2\mathcal{M}_2^\dagger\right) &= C_R^3D_R\times\Big\{\vec{H}^2+R\left(\vec{B}_1^2+\vec{B}_2^2+\vec{C}_1^2+\vec{C}_2^2\right)\\ &+R^2\left(\vec{B}_{2(12)}^2+\vec{C}_{(12)}^2\right)\Big\}+\text{Interference terms}\,.\end{aligned}\tag{75}$$

(See eq. (95) for the full result.) We can isolate the color prefactor together with the leading parabolic dependence $1/k_\perp^2\sim R_g^{(0)}$ in the form

$$R_g^{(2)}(\vec{k},\vec{q}_{1\perp})=R_g^{(0)}(\vec{k})\mathcal{F}^{(2)}(\vec{k}_\perp,\vec{q}_{1\perp},\vec{q}_{2\perp},\xi_1,\xi_2)\,.\tag{76}$$

We note that when the interference terms drop at asymptotic $k_\perp^2\gg2\mu^2$ the enhancement factor scales as in eq. (70)

$$\mathcal{F}^{(2)}(\vec{k}_\perp,\vec{q}_{1\perp},\vec{q}_{2\perp})\ \overset{\vec{k}_\perp^{\,2}\gg2\mu^2}{\longrightarrow}\ (1+R)^2\,.\tag{77}$$

The longitudinal ensemble averaging can be performed in eq. (75) over the times $t_{10}=t_1-t_0\ ,\ t_{21}=t_2-t_1$ as indicated in eqs. (20,39). For the more general case $\lambda_1\neq\lambda_2$ we find

$$\langle\,\cos(\omega_\alpha t_{10}+\omega_\beta t_{21})\,\rangle=\frac{1-\lambda_1\lambda_2\omega_\alpha\omega_\beta}{(1+\lambda_1^2\omega_\alpha^2)(1+\lambda_2^2\omega_\beta^2)}\,.\tag{78}$$

The integration over the momentum transfer due to the rescatterings from the static centers is most readily performed in terms of the dimensionless variables

$$\kappa = \frac{k_\perp^2}{\mu^2}, \quad \theta_i = \frac{q_{i\perp}^2}{\mu^2}, \quad \xi_i = \frac{(t_i - t_{i-1})\mu^2}{2\omega}, \quad i = 1, 2\ , \tag{79}$$

leading to an averaged quantum correction factor

$$\begin{aligned} F^{(2)}(\kappa, \xi_1, \xi_2) &= \left\langle\ \mathcal{F}^{(2)}(\kappa, \vec{q}_{1\perp}, \vec{q}_{2\perp}, \xi_1, \xi_2)\ \right\rangle = \\ &= \int_0^{s/4\mu^2} \frac{d\theta_1}{(\theta_1+1)^2} \frac{d\theta_2}{(\theta_2+1)^2} \int_0^{2\pi} \frac{d\phi_1}{2\pi} \frac{d\phi_2}{2\pi}\, \mathcal{F}^{(2)}\ . \end{aligned} \tag{80}$$

On Fig. 5a we plot the contributions to $\mathcal{F}_{cl}^{(2)}$ – the incoherent parton cascade limit where all the exposed singularities in the propagators have been regulated by the Debye screening mass μ. At small transverse momenta of the radiated gluon the quantum modification is dominated by the "Gunion-Bertsch terms". In the limit of large $k_\perp^2/\mu^2$ the only terms that survive apart from the hard scattering are the "cascade terms". This represents the expected behavior of $R_g^{(2)}(\vec{k}\,)$ in the Bethe-Heitler limit. It is important to notice that simple picture of the process is only possible in the incoherent case where one easily decouples production from rescattering and the separate terms acquire physical interpretation.

Fig. 5b shows $\mathcal{F}^{(2)}$ plotted for the same set of gluon energies ω as in Fig. 4b (and the same values of ξ_i, $i = 1, 2$). The picture of classical parton cascading is modified by the presence of interference terms that control behavior of the probability distribution in the intermediate LPM region. Due to the destructive interference one observes a smooth transition from the "hard term" at small $k_\perp^2$ (i.e. the factorization limit) to the Bethe-Heitler limit.

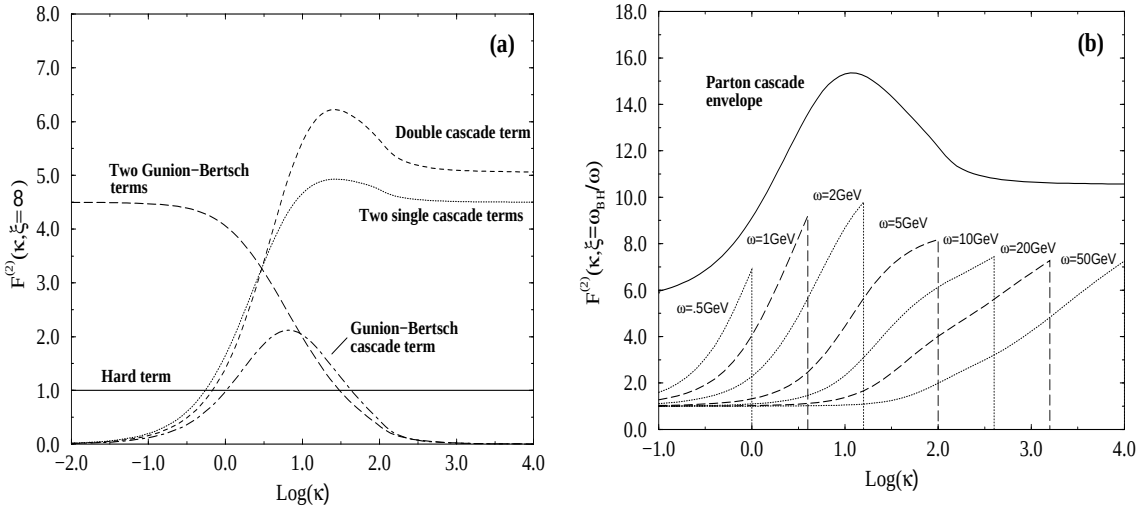

Fig. 5. (a) The structure of the regulated ($\mu = 0.5$ GeV) contributions to the $\xi \to \infty$ limit (quark jet of $E_{jet} = 50$ GeV, $n_s = 2$). (b) Characteristic behavior of $F^{(2)}$ for $\xi = 0.013,\ 0.031,\ 0.063,\ 0.13,\ 0.31,\ 0.63$ and 1.3 .

It is remarkable that the detailed angular profile of the probability distribution is very similar (apart from the explicit rescaling factor) to the one in Fig. 4b.

6 Power Law Scaling in n_s and Estimated Energy Loss

The amplitudes in the case of $n_s = 3$ are tabulated in Appendix C. The main novelty at this order is the appearance of an interesting "color wheel" diagram derived in Appendix D. The amplitude, $\mathcal{M}_3$ is rearranged in eq. (115) in terms of the hard, GB, and cascade amplitudes. The diagonal (classical parton cascade) terms in $|\mathcal{M}_3|^2$ with color factors (117) involve (1) the usual $\vec{H}^2 = 1/k_\perp^2$ with a relative color weight 1, (2) three simple GB induced radiation terms and three one scattering gluon cascade terms each with color weight of $R = C_A/C_R$, (4) three double gluon cascade terms and four GB-cascade terms with a weight R^2, and (5) one triple gluon cascade term with a weight R^3. At small $k_\perp$, only the three simple GB ($\vec{B}^2 \to \vec{H}^2$) terms contribute since the finite cascade terms are negligible relative to the divergent hard and GB terms. In this small $k_\perp$ region therefore the $\vec{H}^2$ term is simply amplified by a factor $1 + 3R$ as illustrated in Fig. 6a. For large angles, on the other hand, all the GB and GB-cascade terms vanish while the cascade terms $\vec{C}^2 \to \vec{H}^2$. Therefore, in that region the hard radiation is amplified by a factor $(1+R)^3$. In between, near $k_\perp \sim \mu$ all terms contribute and a bump that is sensitive to the screening scale μ. Fig. 6a summarizes therefore the general scaling with n_s of the classical parton cascade angular distribution. The power law enhancement $(1 + R)^{n_s}$ at large angles is the most important nonlinear feature since the bump near $\kappa \sim 1$ is killed by destructive interference shown on Fig. 6b.

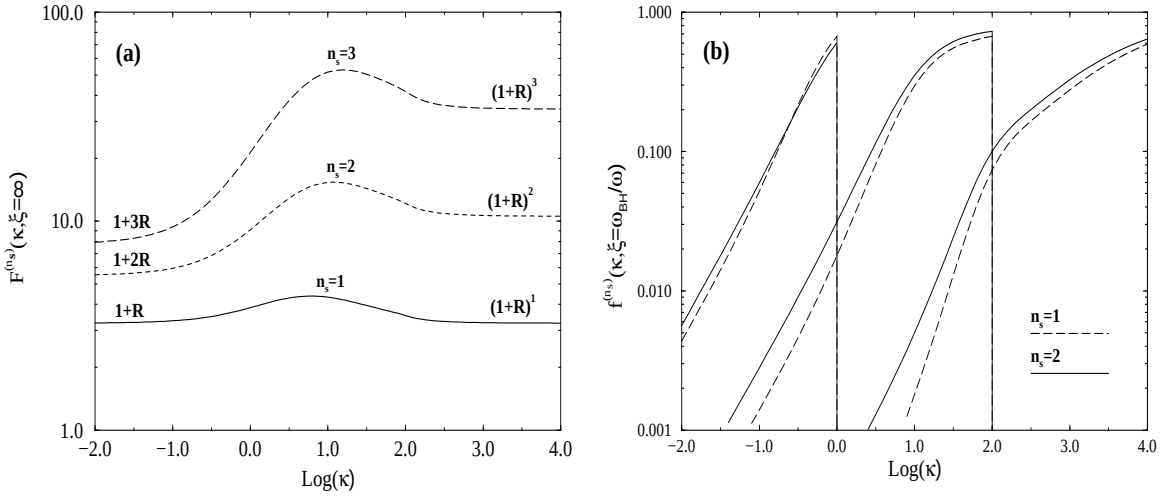

Fig. 6. (a) The classical parton cascade limit ($\xi \to \infty$) angular enhancement factor from eq. (72) for a quark jet ($E_{\rm jet} = 50$ GeV, $\mu = 0.5$ GeV) vs $\log_{10}(k_\perp^2/\mu^2)$. (b) The reduced modification factor $f^{(n_s)}$ including kinematic cut-offs for $n_s = 1, 2$ shows an approximate n_s independence.

In the general case, the small $k_\perp$ enhancement, $1 + n_s R$, expected in the classical cascade limit also is cancelled by destructive interference as seen in Figs. 4 and 5. Here we note a remarkable simple scaling between the $n_s = 1, 2$ cases. In Fig. 6b the reduced modification factors $f^{(n_s)}(\kappa, \xi)$ extracted from $F^{(n_s)}(\kappa, \xi)$ in eq. (72) are shown. The reduced factors are nearly identical in spite of the much more complex functional form of the $R_g^{(2)}$ than $R_g^{(1)}$.

The approximate scaling from $n_s = 1$ to $n_s = 2$ can be summarized as follows:

$$R_g^{(n_s)}(\omega, \vec{k}_\perp) \approx R_g^{(0)}(k_\perp) \left\{1 + ((1+R)^{n_s} - 1)\ f^{(1)}(\kappa, \xi)\right\} . \tag{81}$$

The generic analytic structure of the reduced modification factor can be roughly approximated by $f^{(1)}(\kappa, \xi) \sim \kappa^2\xi^2/(1 + \kappa^2\xi^2)$, which shows that the classical parton cascade result is approached only for $\kappa > 1/\xi$, i.e., $k_\perp > \sqrt{\omega/\lambda}$ For higher n_s the validity of this scaling will be tested in [12].

Here we extrapolate eq. (81) to $n_s = 3$ to make a rough estimate of the energy loss spectrum $dI/d\omega$ and the fractional energy loss $\Delta E/E$ to $L \sim 3$ fm. We emphasize that these estimates are included in this paper only to illustrate qualitative features. For quantitative estimates, multi-gluon showers that require a Monte Carlo analysis must be considered as deferred to ref. [12]. The normalization factor $Z_{n_s} \gg 1$ for even modest $n_s \sim 3$ in eq. (47) signals a high probability of multi-gluon emission. This is well known in the $n_s = 0$ case as emphasized in eqs. (48,49). For example, $Z_0 > 2$ from eq. (48) for $E > 10$ GeV while DLA gives, $Z_0 \approx 3$. Eq. (49) then leads to $\langle n_g \rangle \approx 1.2$ for this energy, implying that two gluon final states must be taken into account.

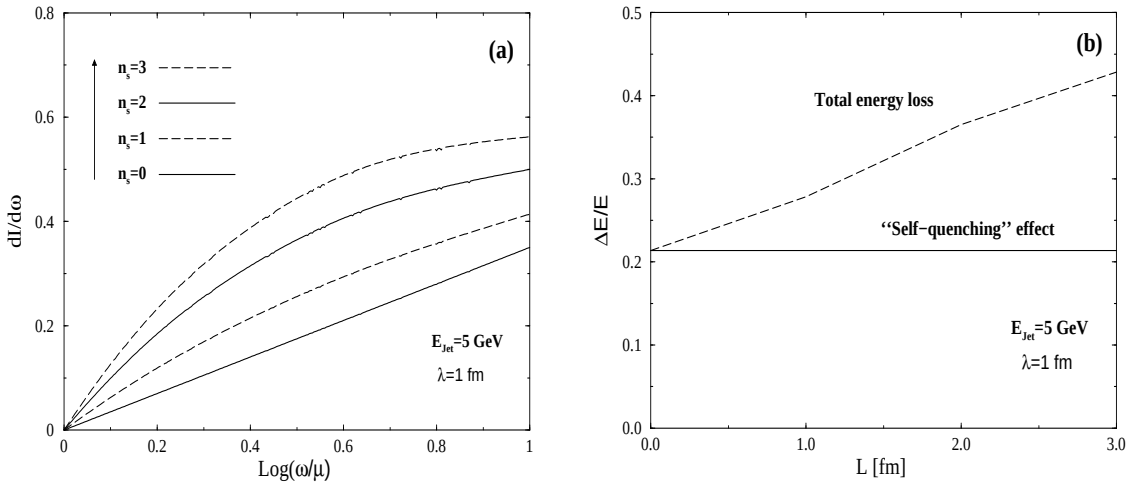

Fig. 7. (a) The gluon radiation intensity dI/dw for a 5 GeV quark jet ($n_s = 0, 1, 2, 3$) based on (81) is illustrated. (b) The fractional energy loss is shown for the "self-quenching" and medium modified cases.

With the above caveats, Fig. 7 illustrates the qualitative features of the angular integrated $dI/d\omega$ and $\Delta E/E$ for a quark jet of energy 5 GeV penetrating a thin ($n_s = 1, 2, 3$) plasma with $\mu = 0.5$ GeV, $\lambda = 1$ fm, $\alpha_s = 0.3$. As seen from eq. (15), the intensity distribution for the self-quenching ($n_s = 0$) case increases linearly as a

function of $\log(\omega/\mu)$ and the fractional energy loss due to self-quenching is proportional to $\log(E/\mu)$.

With increasing n_s, the approximate scaling in eq. (81) leads to:

$$\omega\frac{dN_g^{(n_s,n_g=1)}}{d^3\,\vec{k}} \approx \frac{1}{Z_{n_s}}\frac{C_R\alpha_s}{\pi^2}\frac{1}{k_\perp^2}\left\{1+((1+R)^{n_s}-1)f^{(1)}(\kappa,\xi)\right\}\ ,$$

$$Z_{n_s} \approx 1+\frac{C_R\alpha_s}{\pi}\int_\mu^E\frac{d\omega}{\omega}\int_{\mu^2}^{\omega^2}\frac{dk_\perp^2}{k_\perp^2}\left\{1+((1+R)^{n_s}-1)f^{(1)}\left(\frac{k_\perp^2}{\mu^2},\frac{\omega_{BH}}{\omega}\right)\right\}\ . \qquad (82)$$

Without the Z factor, the gluon distribution would scale approximately exponentially with plasma thickness at high $k_\perp > \mu/\sqrt{\xi}$ due to the multiple collisions of the gluon in the target. However, the normalization factor compensates this increase to a very large extent as seen in Fig. 7. In fact, at this single gluon level of approximation, the energy loss is surprisingly small, ~ 300 MeV/fm, and only grows approximately linearly with increasing thickness $L = n_s\lambda$ in spite of the large modification of the gluon angular distribution.

7 Summary

We investigated the angular distribution of radiated gluons and the energy loss of hard jet in thin plasmas, where the size of the plasma L is comparable to the the mean free path, λ. The small number of rescattering terms made it possible to calculate analytically the full matrix element within the eikonal approximation. This paper established a systematic method for computation of all relevant partonic matrix elements for higher n_s which are needed as input to a numerical Monte-Carlo study of the actual hadronic observables associated with jet quenching to be presented in a subsequent paper [12]. We developed an efficient algorithm to automate the cumbersome color algebra and keep track of the many canceling phases involved in the non-abelian Landau-Pomeranchuk-Migdal effect. Detailed discussion for the $n_s = 1, 2, 3$ cases were presented to clarify the how the competing physical processes interfere in different kinematic regions. An approximate power law scaling of the angular broadening emerged with the increasing number of the rescattering centers. However, the rapidly growing wavefunction renormalization was shown to limit the growth of final energy loss. For quantitative comparison with data, multigluon emission will be shown in GLV II[12] to dominate the jet quenching pattern at the observable hadronic level.

Acknowledgments

We thank Urs Wiedemann for extensive discussions related to this problem. This work was supported by the DOE Research Grant under Contract No. De-FG-02-92ER-40764, partly by the US-Hungarian Joint Fund No.652 and OTKA No. T025579.

A Case of Two Scattering Centers

In the approximation of a high energy incident parton and soft gluon bremsstrahlung the seven planar diagrams in Fig. 8 can be treated in the eikonal approximation spinless limit.

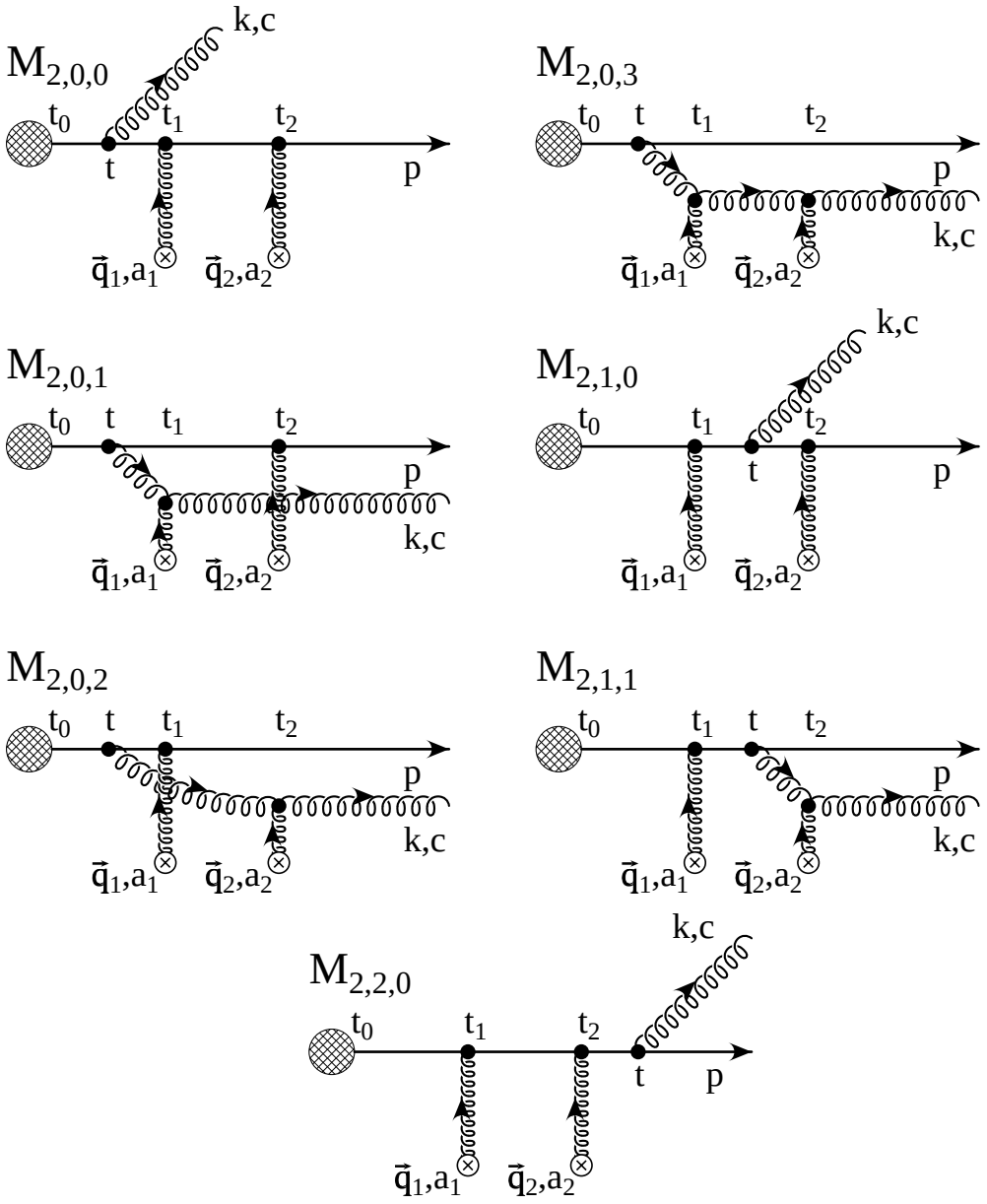

Fig. 8. The contributions to $M_J \otimes M_2$ soft gluon radiation amplitude in case of two scatterings.

We denote by t_0 the time at which the particle is produced in the medium and by $t_i,\ i = 1, 2$ the times of the successive rescatterings. In the approximation when $\lambda \gg \mu^{-1}$ "backward" scattering can be neglected and the process is approximately time

ordered [9]. We denote by $\vec{k}$ the momentum of the radiated gluon and by $\vec{q}_i,\ i=1,2$ are the momentum transfers. In QCD with each vertex we associate a generator of the $SU(3)$ group. We denote them by c for the radiated gluon and $a_i,\ i=1,2$ for the momentum transfer vertices. The polarization of the radiated gluon is determined by $\vec{\epsilon}_\perp$.

The corresponding amplitudes can be obtained with the procedure described in eqs. (30,33-35):

$$\mathcal{M}_{2,0,0} = 2ig_s\frac{\vec{\epsilon}_\perp\cdot\vec{k}_\perp}{k_\perp^2}(e^{it_1\frac{k_\perp^2}{2\omega}}-e^{it_0\frac{k_\perp^2}{2\omega}})a_2a_1c \ , \tag{83}$$

$$\mathcal{M}_{2,0,1} = 2ig_s\frac{\vec{\epsilon}_\perp\cdot(\vec{k}-\vec{q}_1)_\perp}{(k-q_1)_\perp^2}e^{it_1\frac{k_\perp^2-(k-q_1)_\perp^2}{2\omega}}\times$$
$$\times(e^{it_1\frac{(k-q_1)_\perp^2}{2\omega}}-e^{it_0\frac{(k-q_1)_\perp^2}{2\omega}})a_2\left[c,a_1\right] \ , \tag{84}$$

$$\mathcal{M}_{2,0,2} = 2ig_s\frac{\vec{\epsilon}_\perp\cdot(\vec{k}-\vec{q}_2)_\perp}{(k-q_2)_\perp^2}e^{it_2\frac{k_\perp^2-(k-q_2)_\perp^2}{2\omega}}\times$$
$$\times(e^{it_1\frac{(k-q_2)_\perp^2}{2\omega}}-e^{it_0\frac{(k-q_2)_\perp^2}{2\omega}})a_1\left[c,a_2\right] \ , \tag{85}$$

$$\mathcal{M}_{2,0,3} = 2ig_s\frac{\vec{\epsilon}_\perp\cdot(\vec{k}-\vec{q}_1-\vec{q}_2)_\perp}{(k-q_1-q_2)_\perp^2}e^{it_2\frac{k_\perp^2-(k-q_2)_\perp^2}{2\omega}}e^{it_1\frac{(k-q_2)_\perp^2-(k-q_1-q_2)_\perp^2}{2\omega}}\times$$
$$\times(e^{it_1\frac{(k-q_1-q_2)_\perp^2}{2\omega}}-e^{it_0\frac{(k-q_1-q_2)_\perp^2}{2\omega}})\left[\left[c,a_2\right],a_1\right] \ , \tag{86}$$

$$\mathcal{M}_{2,1,0} = 2ig_s\frac{\vec{\epsilon}_\perp\cdot\vec{k}_\perp}{k_\perp^2}(e^{it_2\frac{k_\perp^2}{2\omega}}-e^{it_1\frac{k_\perp^2}{2\omega}})a_2ca_1 \ , \tag{87}$$

$$\mathcal{M}_{2,1,1} = 2ig_s\frac{\vec{\epsilon}_\perp\cdot(\vec{k}-\vec{q}_2)_\perp}{(k-q_2)_\perp^2}e^{it_2\frac{k_\perp^2-(k-q_2)_\perp^2}{2\omega}}\times$$
$$\times(e^{it_2\frac{(k-q_2)_\perp^2}{2\omega}}-e^{it_1\frac{(k-q_2)_\perp^2}{2\omega}})\left[c,a_2\right]a_1 \ , \tag{88}$$

$$\mathcal{M}_{2,2,0} = 2ig_s\frac{\vec{\epsilon}_\perp\cdot\vec{k}_\perp}{k_\perp^2}(-e^{it_2\frac{k_\perp^2}{2\omega}})ca_2a_1 \ . \tag{89}$$

After regrouping the sum of the above amplitudes five distinct color factors remain in eq. (73). We label them as follows:

$$\mathcal{C}_1=a_2a_1c\ ,\quad \mathcal{C}_2=a_2\left[c,a_1\right]\ ,\quad \mathcal{C}_3=\left[c,a_2\right]a_1\ ,$$
$$\mathcal{C}_4=a_1\left[c,a_2\right]\ ,\quad \mathcal{C}_5=\left[\left[c,a_2\right],a_1\right]\ . \tag{90}$$

In the case of QCD the "color" and "kinematic" parts of a diagram factor. Diagrammatic techniques have been developed to treat the color part alone [25].

We denote by C_R the Casimir of the representation of the incident parton. For $SU(N)$ following the standard normalization for the generators we have

$$C_F=\frac{N^2-1}{2N},\qquad C_A=N. \tag{91}$$

The trace of the color factors can be taken separately in the square of the matrix element, yielding

Diagonal part:

$$\begin{aligned}
&\mathrm{Tr}\,\mathcal{C}_1\mathcal{C}_1^\dagger = C_R^3 D_R\ ,\\
&\mathrm{Tr}\,\mathcal{C}_2\mathcal{C}_2^\dagger = \mathrm{Tr}\,\mathcal{C}_3\mathcal{C}_3^\dagger = \mathrm{Tr}\,\mathcal{C}_4\mathcal{C}_4^\dagger = C_A C_R^2 D_R\ ,\\
&\mathrm{Tr}\,\mathcal{C}_5\mathcal{C}_5^\dagger = C_A^2 C_R D_R\ .
\end{aligned} \tag{92}$$

Off-diagonal part:

$$\begin{aligned}
&\mathrm{Tr}\,\mathcal{C}_1\mathcal{C}_2^\dagger = -\tfrac{1}{2} C_A C_R^2 D_R\ ,\\
&\mathrm{Tr}\,\mathcal{C}_1\mathcal{C}_3^\dagger = \mathrm{Tr}\,\mathcal{C}_1\mathcal{C}_4^\dagger = -\tfrac{1}{2}\left(C_R - \tfrac{1}{2}C_A\right) C_A C_R D_R\ ,\\
&\mathrm{Tr}\,\mathcal{C}_2\mathcal{C}_3^\dagger = \mathrm{Tr}\,\mathcal{C}_2\mathcal{C}_5^\dagger = -\tfrac{1}{4} C_A^2 C_R D_R\ ,\\
&\mathrm{Tr}\,\mathcal{C}_3\mathcal{C}_4^\dagger = -\mathrm{Tr}\,\mathcal{C}_4\mathcal{C}_5^\dagger = \left(C_R - \tfrac{1}{2}C_A\right) C_A C_R D_R\ ,\\
&\mathrm{Tr}\,\mathcal{C}_3\mathcal{C}_5^\dagger = \tfrac{1}{2} C_A^2 C_R\ .
\end{aligned} \tag{93}$$

Diagrams with 0:

$$\mathrm{Tr}\,\mathcal{C}_1\mathcal{C}_5^\dagger = \mathrm{Tr}\,\mathcal{C}_2\mathcal{C}_4^\dagger = 0\ . \tag{94}$$

With $R = C_A/C_R$, the relative conditional probability is given by

$$\begin{aligned}
R_g^{(2)}(\vec{k}\,) \;=\; & \frac{\alpha_s}{\pi^2} C_R \left\{ \vec{H}^2 + R\left(\vec{B}_1^2 + \vec{B}_2^2 + \vec{C}_1^2 + \vec{C}_2^2\right) + R^2\left(\vec{B}_{2(12)}^2 + \vec{C}_{(12)}^2\right)\right.\\
& - R\,(\frac{R}{2})\,\vec{B}_1\cdot\vec{B}_2\cos(t_{21}\omega_0) - R\,(\frac{R}{2})\,\vec{C}_1\cdot\vec{B}_2\cos(t_{21}\omega_0 + t_{10}\omega_1)\\
& + 2R^2\,\vec{C}_{(12)}\cdot\vec{B}_{2(12)}\cos(t_{10}\omega_{(12)}) - R\left(\vec{H}\cdot\vec{B}_1\cos(t_{10}\omega_0)\right.\\
& \left. + \vec{H}\cdot\vec{C}_1\cos(t_{10}\omega_{10}) - 2\vec{C}_1\cdot\vec{B}_1\cos(t_{10}\omega_1)\right)\\
& - R\,(1 - \frac{R}{2})\left(\vec{H}\cdot\vec{B}_2\cos(t_{20}\omega_0) + \vec{H}\cdot\vec{C}_2\cos(t_{20}\omega_{20})\right.\\
& \left. - 2\vec{C}_2\cdot\vec{B}_2\cos(t_{20}\omega_2)\right) - R\,(\frac{R}{2})\left(\vec{C}_1\cdot\vec{B}_{2(12)}\cos(t_{10}\omega_1 - t_{21}\omega_{20})\right.\\
& + \vec{C}_1\cdot\vec{C}_{(12)}\cos(t_{10}\omega_{1(12)} - t_{21}\omega_{20}) + \vec{B}_1\cdot\vec{B}_{2(12)}\cos(t_{21}\omega_{20})\\
& \left. + \vec{B}_1\cdot\vec{C}_{(12)}\cos(t_{10}\omega_{(12)} + t_{21}\omega_{20})\right) - R^2\left(\vec{C}_2\cdot\vec{B}_{2(12)}\cos(t_{10}\omega_2)\right.\\
& + \vec{C}_2\cdot\vec{C}_{(12)}\cos(t_{10}\omega_{2(12)}) - \vec{B}_2\cdot\vec{B}_{2(12)}\cos(t_{21}\omega_2)\\
& \left.\left. - \vec{B}_2\cdot\vec{C}_{(12)}\cos(t_{10}\omega_{(12)} + t_{21}\omega_2)\right)\right\}\ ,
\end{aligned} \tag{95}$$

where we have used the concise notation introduced in Sec. 4.

B The $t_0 \to -\infty$ Limit in the Case of $n_s = 2$

Going back to eq. (73) it is easy to check the $t_0 \to -\infty$ limit and make contact with BDMPS [9]. In the phases we will assume small adiabatic switch-off factors $\pm i\varepsilon$ when

taking the corresponding limits.

The limit of $t_0 \to -\infty$ corresponds to removing the interference with the jet source. In this limit only the two Gunion-Bertsch terms and the Gunion-Bertsch cascade term survive.

$$\begin{aligned}\mathcal{M}_2 &= -2ig_s\,\vec{\epsilon}_\perp\cdot\Big\{\vec{B}_1 e^{it_1\omega_0}a_2\,[c,a_1]+\vec{B}_2 e^{it_2\omega_0}\,[c,a_2]\,a_1 \\ &\quad +\vec{B}_{2(12)}e^{i(t_2\omega_0-t_{21}\omega_2)}\,[[c,a_2],a_1]\Big\}\ . \end{aligned} \tag{96}$$

This is the two-scattering generalization of the Gunion-Bertsch one scattering center formula [6] and corresponds exactly to eq. (2.22) of BDMPS [9]. However, when squared there are several extra terms compared to the *one effective term* retained in the approximations employed there. In particular, from eq. (95)

$$\begin{aligned}&\lim_{t_0\to-\infty}\omega\frac{dN_g^{(2)}}{d\omega}=\int d^2\vec{k}_\perp\frac{dN_g^{(2)}}{dyd^2\vec{k}_\perp}=\frac{\alpha_s}{\pi^2}C_A\Big\langle\int d^2\vec{k}_\perp\ \Big\{\vec{B}_1^2+\vec{B}_2^2 \\ &+R\,\vec{B}_{2(12)}^2-\left(\frac{R}{2}\right)\Big(\vec{B}_1\cdot\vec{B}_2\cos(t_{21}\omega_0)+\vec{B}_1\cdot\vec{B}_{2(12)}\cos(t_{21}\omega_{20}) \\ &-2\,\vec{B}_2\cdot\vec{B}_{2(12)}\cos(t_{21}\omega_2)\Big)\Big\}\Big\rangle\ . \end{aligned} \tag{97}$$

After taking the kinematic limits to infinity and performing the substitution $\vec{k}_\perp = \vec{k}'_\perp - \vec{q}_{2\perp}$ in the $\vec{B}_1\cdot\vec{B}_2$ contribution one arrives at a result that in the large N_c limit, i.e. $R=2$, the weighted energy distribution of the gluons has the form:

$$\begin{aligned}\lim_{t_0\to-\infty}\omega\frac{dN_g^{(2)}}{d\omega} &= \omega\frac{dN_g^{(2)fact.}}{d\omega} \\ &+ 3\frac{\alpha_s}{\pi^2}C_A\left\langle\int d^2\vec{k}_\perp\ \Big(\vec{B}_2\cdot\vec{B}_{2(12)}\left(\cos(t_{21}\omega_2)-1\right)\Big)\right\rangle \\ &- \frac{\alpha_s}{\pi^2}C_A\left\langle\int d^2\vec{k}_\perp\ \Big(\vec{B}_1\cdot\vec{B}_{2(12)}\left(\cos(t_{21}\omega_{20})-1\right)\Big)\right\rangle \\ &= \omega\frac{dN_g^{(2)fact.}}{d\omega}+\omega\frac{dN_g^{(2)BDMPS}}{d\omega} \\ &- \frac{\alpha_s}{\pi^2}C_A\left\langle\int d^2\vec{k}_\perp\ \Big(\vec{B}_1\cdot\vec{B}_{2(12)}\left(\cos(t_{21}\omega_{20})-1\right)\Big)\right\rangle\ , \end{aligned} \tag{98}$$

where direct comparison to eq. (2.31) in Ref. [9] shows that

$$\begin{aligned}\omega\frac{dN_{BDMPS}^{(2)}}{d\omega} &= 3\frac{C_A\alpha_s}{\pi^2}\left\langle\int d^2\vec{k}\ \left(\frac{(\vec{k}-\vec{q}_2)_\perp}{(k-q_2)_\perp^2}-\frac{(\vec{k}-\vec{q}_1-\vec{q}_2)_\perp}{(k-q_1-q_2)_\perp^2}\right)\cdot\right. \\ &\quad\left.\cdot\left(\frac{\vec{k}_\perp}{k_\perp^2}-\frac{(\vec{k}-\vec{q}_2)_\perp}{(k-q_2)_\perp^2}\right)\left(\cos(t_{21}\omega_2)-1\right)\right\rangle \\ &= 3\frac{C_A\alpha_s}{\pi^2}\left\langle\int d^2\vec{k}\ \langle\vec{B}_2\cdot\vec{B}_{2(12)}(\cos(t_{21}\omega_2)-1)\right\rangle\ . \end{aligned} \tag{99}$$

If we also require that $t_2-t_1\to\infty$ then the Gunion-Bertsch cascade term is also vanishes and we reproduce two independent Gunion-Bertsch scatterings with gluon radiation.

C Case of Three Scattering Centers

The interaction of the incident high energy parton with three scattering centers accompanied by emission of one gluon is described (in the eikonal approach) by the following fifteen diagrams:

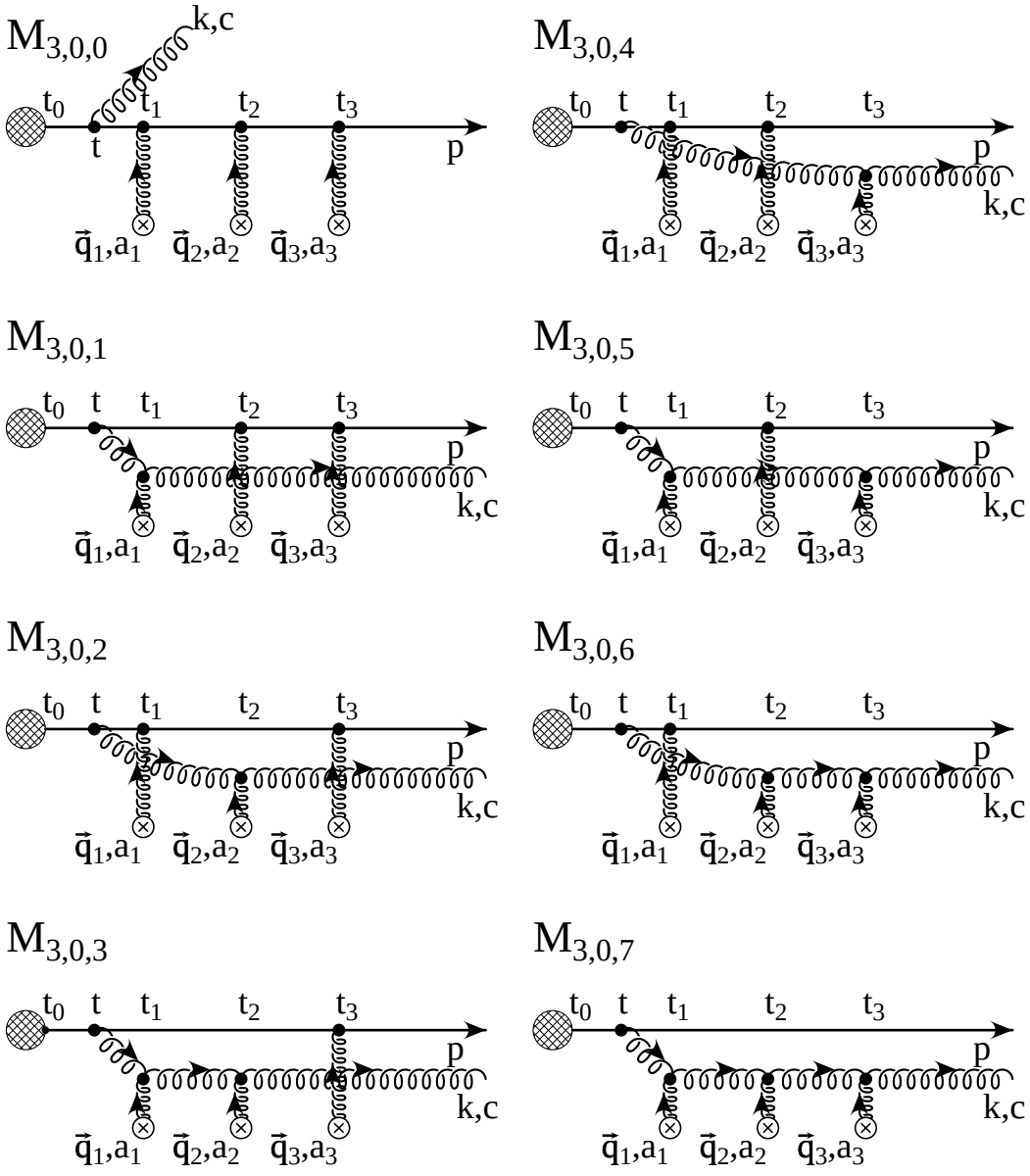

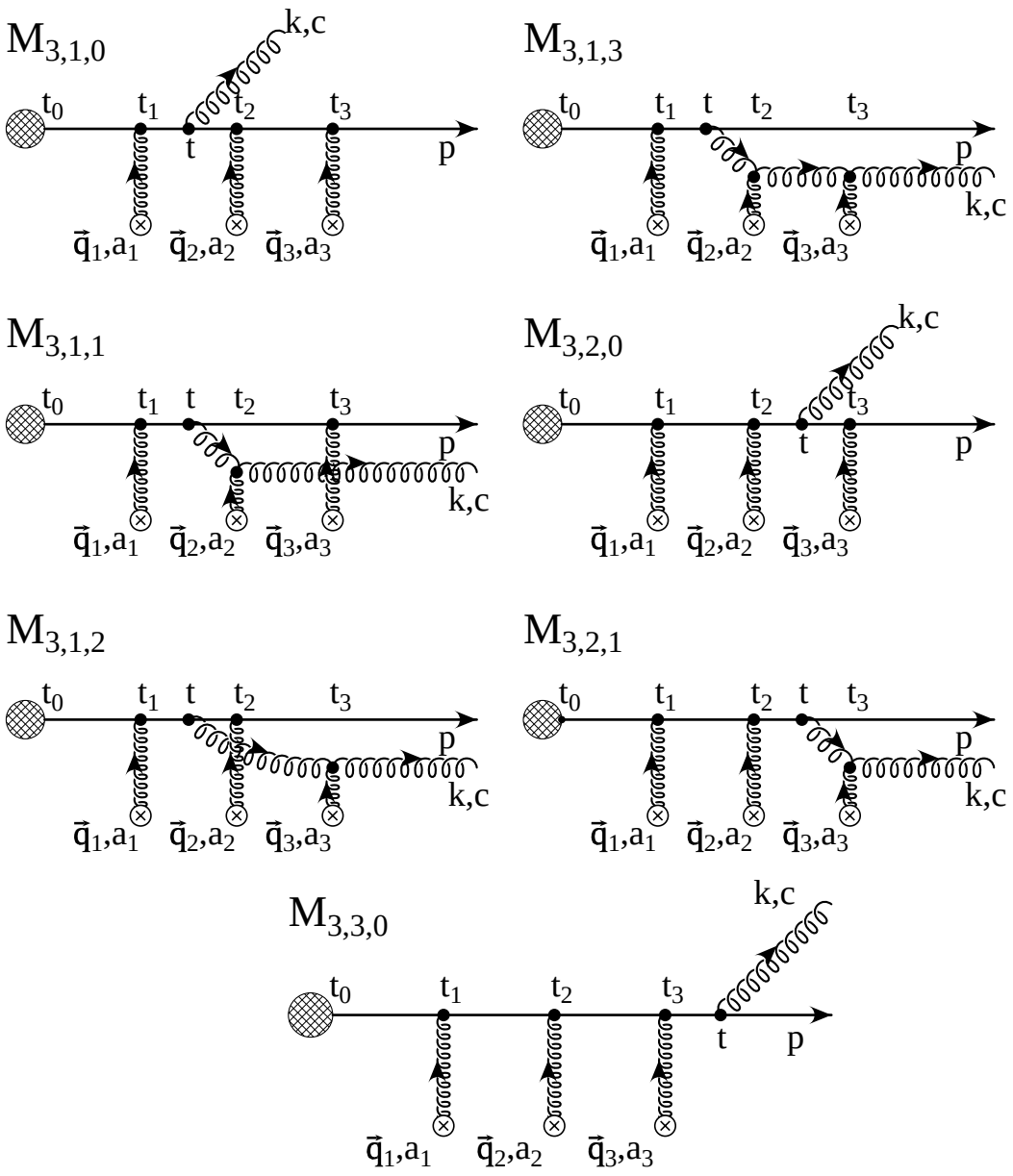

Fig. 9. The contributions to $M_J \otimes M_3$ soft gluon radiation amplitude in case of three scatterings.

The corresponding matrix elements are easy to obtain through the procedure described in Sec. 3.3

$$\mathcal{M}_{3,0,0} \;=\; 2ig_s \frac{\vec{\epsilon}_\perp \cdot \vec{k}_\perp}{k_\perp^2} (e^{it_1 \frac{k_\perp^2}{2\omega}} - e^{it_0 \frac{k_\perp^2}{2\omega}}) a_3 a_2 a_1 c \;, \tag{100}$$

$$
\begin{aligned}
\mathcal{M}_{3,0,1} &= 2ig_s\frac{\vec{\epsilon}_\perp\cdot(\vec{k}-\vec{q}_1)_\perp}{(k-q_1)_\perp^2}e^{it_1\frac{k_\perp^2-(k-q_1)_\perp^2}{2\omega}}\times \\
&\quad\times(e^{it_1\frac{(k-q_1)_\perp^2}{2\omega}}-e^{it_0\frac{(k-q_1)_\perp^2}{2\omega}})a_3a_2\left[c,a_1\right]\ , && (101)\\
\mathcal{M}_{3,0,2} &= 2ig_s\frac{\vec{\epsilon}_\perp\cdot(\vec{k}-\vec{q}_2)_\perp}{(k-q_2)_\perp^2}e^{it_2\frac{k_\perp^2-(k-q_2)_\perp^2}{2\omega}}\times \\
&\quad\times(e^{it_1\frac{(k-q_2)_\perp^2}{2\omega}}-e^{it_0\frac{(k-q_2)_\perp^2}{2\omega}})a_3a_1\left[c,a_2\right]\ , && (102)\\
\mathcal{M}_{3,0,3} &= 2ig_s\frac{\vec{\epsilon}_\perp\cdot(\vec{k}-\vec{q}_1-\vec{q}_2)_\perp}{(k-q_1-q_2)_\perp^2}e^{it_2\frac{k_\perp^2-(k-q_2)_\perp^2}{2\omega}}e^{it_1\frac{(k-q_2)_\perp^2-(k-q_1-q_2)_\perp^2}{2\omega}}\times \\
&\quad\times(e^{it_1\frac{(k-q_1-q_2)_\perp^2}{2\omega}}-e^{it_0\frac{(k-q_1-q_2)_\perp^2}{2\omega}})a_3\left[\left[c,a_2\right],a_1\right]\ , && (103)\\
\mathcal{M}_{3,0,4} &= 2ig_s\frac{\vec{\epsilon}_\perp\cdot(\vec{k}-\vec{q}_3)_\perp}{(k-q_3)_\perp^2}e^{it_3\frac{k_\perp^2-(k-q_3)_\perp^2}{2\omega}}\times \\
&\quad\times(e^{it_1\frac{(k-q_3)_\perp^2}{2\omega}}-e^{it_0\frac{(k-q_3)_\perp^2}{2\omega}})a_2a_1\left[c,a_3\right]\ , && (104)\\
\mathcal{M}_{3,0,5} &= 2ig_s\frac{\vec{\epsilon}_\perp\cdot(\vec{k}-\vec{q}_1-\vec{q}_3)_\perp}{(k-q_1-q_3)_\perp^2}e^{it_3\frac{k_\perp^2-(k-q_3)_\perp^2}{2\omega}}e^{it_1\frac{(k-q_3)_\perp^2-(k-q_1-q_3)_\perp^2}{2\omega}}\times \\
&\quad\times(e^{it_1\frac{(k-q_1-q_3)_\perp^2}{2\omega}}-e^{it_0\frac{(k-q_1-q_3)_\perp^2}{2\omega}})a_2\left[\left[c,a_3\right],a_1\right]\ , && (105)\\
\mathcal{M}_{3,0,6} &= 2ig_s\frac{\vec{\epsilon}_\perp\cdot(\vec{k}-\vec{q}_2-\vec{q}_3)_\perp}{(k-q_2-q_3)_\perp^2}e^{it_3\frac{k_\perp^2-(k-q_3)_\perp^2}{2\omega}}e^{it_2\frac{(k-q_3)_\perp^2-(k-q_2-q_3)_\perp^2}{2\omega}}\times \\
&\quad\times(e^{it_1\frac{(k-q_2-q_3)_\perp^2}{2\omega}}-e^{it_0\frac{(k-q_2-q_3)_\perp^2}{2\omega}})a_1\left[\left[c,a_3\right],a_2\right]\ , && (106)\\
\mathcal{M}_{3,0,7} &= 2ig_s\frac{\vec{\epsilon}_\perp\cdot(\vec{k}-\vec{q}_1-\vec{q}_2-\vec{q}_3)_\perp}{(k-q_1-q_2-q_3)_\perp^2}e^{it_3\frac{k_\perp^2-(k-q_3)_\perp^2}{2\omega}}\times \\
&\quad\times e^{it_2\frac{(k-q_3)_\perp^2-(k-q_2-q_3)_\perp^2}{2\omega}}e^{it_1\frac{(k-q_2-q_3)_\perp^2-(k-q_1-q_2-q_3)_\perp^2}{2\omega}}\times \\
&\quad\times(e^{it_1\frac{(k-q_1-q_2-q_3)_\perp^2}{2\omega}}-e^{it_0\frac{(k-q_1-q_2-q_3)_\perp^2}{2\omega}})\left[\left[\left[c,a_3\right],a_2\right],a_1\right]\ , && (107)\\
\mathcal{M}_{3,1,0} &= 2ig_s\frac{\vec{\epsilon}_\perp\cdot\vec{k}_\perp}{k_\perp^2}(e^{it_2\frac{k_\perp^2}{2\omega}}-e^{it_1\frac{k_\perp^2}{2\omega}})a_3a_2ca_1\ , && (108)\\
\mathcal{M}_{3,1,1} &= 2ig_s\frac{\vec{\epsilon}_\perp\cdot(\vec{k}-\vec{q}_2)_\perp}{(k-q_2)_\perp^2}e^{it_2\frac{k_\perp^2-(k-q_2)_\perp^2}{2\omega}}\times \\
&\quad\times(e^{it_2\frac{(k-q_2)_\perp^2}{2\omega}}-e^{it_1\frac{(k-q_2)_\perp^2}{2\omega}})a_3\left[c,a_2\right]a_1\ , && (109)\\
\mathcal{M}_{3,1,2} &= 2ig_s\frac{\vec{\epsilon}_\perp\cdot(\vec{k}-\vec{q}_3)_\perp}{(k-q_3)_\perp^2}e^{it_2\frac{k_\perp^2-(k-q_3)_\perp^2}{2\omega}}\times \\
&\quad\times(e^{it_2\frac{(k-q_3)_\perp^2}{2\omega}}-e^{it_1\frac{(k-q_3)_\perp^2}{2\omega}})a_2\left[c,a_3\right]a_1\ , && (110)
\end{aligned}
$$

$$
\begin{aligned}
\mathcal{M}_{3,1,3} &= 2ig_s \frac{\vec{\epsilon}_\perp \cdot (\vec{k} - \vec{q}_2 - \vec{q}_3)_\perp}{(k - q_2 - q_3)_\perp^2} e^{it_3 \frac{k_\perp^2 - (k-q_3)_\perp^2}{2\omega}} e^{it_2 \frac{(k-q_3)_\perp^2 - (k-q_2-q_3)_\perp^2}{2\omega}} \times \\
&\quad \times (e^{it_2 \frac{(k-q_2-q_3)_\perp^2}{2\omega}} - e^{it_1 \frac{(k-q_2-q_3)_\perp^2}{2\omega}}) \left[[c, a_3], a_2 \right] a_1 \ , \qquad (111) \\
\mathcal{M}_{3,2,0} &= 2ig_s \frac{\vec{\epsilon}_\perp \cdot \vec{k}_\perp}{k_\perp^2} (e^{it_3 \frac{k_\perp^2}{2\omega}} - e^{it_2 \frac{k_\perp^2}{2\omega}}) a_3 c a_2 a_1 \ , \qquad (112) \\
\mathcal{M}_{3,2,1} &= 2ig_s \frac{\vec{\epsilon}_\perp \cdot (\vec{k} - \vec{q}_3)_\perp}{(k - q_3)_\perp^2} e^{it_3 \frac{k_\perp^2 - (k-q_3)_\perp^2}{2\omega}} \times \\
&\quad \times (e^{it_3 \frac{(k-q_3)_\perp^2}{2\omega}} - e^{it_2 \frac{(k-q_3)_\perp^2}{2\omega}}) \left[c, a_3 \right] a_2 a_1 \ , \qquad (113) \\
\mathcal{M}_{3,3,0} &= 2ig_s \frac{\vec{\epsilon}_\perp \cdot \vec{k}_\perp}{k_\perp^2} (-e^{it_3 \frac{k_\perp^2}{2\omega}}) c a_3 a_2 a_1 \ . \qquad (114)
\end{aligned}
$$

Organizing the sum of the matrix elements in groups with common color and phase factors we obtain

$$
\begin{aligned}
\mathcal{M}_3 &= -2ig_s e^{it_0\omega_0} \times \vec{\epsilon}_\perp \cdot \Big\{ \vec{H} a_3 a_2 a_1 c + \vec{B}_1 e^{it_{10}\omega_0} a_3 a_2 \left[c, a_1 \right] \\
&\quad + \vec{B}_2 e^{it_{20}\omega_0} a_3 \left[c, a_2 \right] a_1 + \vec{B}_3 e^{it_{30}\omega_0} \left[c, a_3 \right] a_2 a_1 \\
&\quad + \vec{B}_{2(12)} e^{i(t_{20}\omega_0 - t_{21}\omega_2)} a_3 \left[\left[c, a_2 \right], a_1 \right] \\
&\quad + \vec{B}_{3(13)} e^{i(t_{30}\omega_0 - t_{31}\omega_3)} a_2 \left[\left[c, a_3 \right], a_1 \right] \\
&\quad + \vec{B}_{3(23)} e^{i(t_{30}\omega_0 - t_{32}\omega_3)} \left[\left[c, a_3 \right], a_2 \right] a_1 \\
&\quad + \vec{B}_{(23)(123)} e^{-i(t_{32}\omega_{30} + t_{21}\omega_{(23)0} + t_{10}\omega_0)} \left[\left[\left[c, a_3 \right], a_2 \right], a_1 \right] \\
&\quad + \vec{C}_1 e^{-it_{10}\omega_{10}} a_3 a_2 \left[c, a_1 \right] + \vec{C}_2 e^{-it_{20}\omega_{20}} a_3 a_1 \left[c, a_2 \right] \\
&\quad + \vec{C}_3 e^{-it_{30}\omega_{30}} a_2 a_1 \left[c, a_3 \right] \\
&\quad + \vec{C}_{(12)} e^{-i(t_{10}\omega_{(12)0} + t_{21}\omega_{20})} a_3 \left[\left[c, a_2 \right], a_1 \right] \\
&\quad + \vec{C}_{(13)} e^{-i(t_{10}\omega_{(13)0} + t_{31}\omega_{30})} a_2 \left[\left[c, a_3 \right], a_1 \right] \\
&\quad + \vec{C}_{(23)} e^{-i(t_{20}\omega_{(23)0} + t_{32}\omega_{30})} a_1 \left[\left[c, a_3 \right], a_2 \right] \\
&\quad + \vec{C}_{(123)} e^{-i(t_{32}\omega_{30} + t_{21}\omega_{(23)0} - t_{10}\omega_{(123)0})} \left[\left[\left[c, a_3 \right], a_2 \right], a_1 \right] \Big\} \ . \qquad (115)
\end{aligned}
$$

Eleven distinct color factors are present for $n_s = 3$. We label them as follows:

$$
\begin{aligned}
&\mathcal{C}_1 = a_3 a_2 a_1 c \ , && \mathcal{C}_2 = a_3 a_2 \left[c, a_1 \right] \ , && \mathcal{C}_3 = a_3 \left[c, a_2 \right] a_1 \ , \\
&\mathcal{C}_4 = \left[c, a_3 \right] a_2 a_1 \ , && \mathcal{C}_5 = a_3 a_1 \left[c, a_2 \right] \ , && \mathcal{C}_6 = a_2 a_1 \left[c, a_3 \right] \ , \\
&\mathcal{C}_7 = a_3 \left[\left[c, a_2 \right], a_1 \right] \ , && \mathcal{C}_8 = a_2 \left[\left[c, a_3 \right], a_1 \right] \ , && \mathcal{C}_9 = \left[\left[c, a_3 \right] a_2 \right] a_1 \ , \\
&\mathcal{C}_{10} = a_1 \left[\left[c, a_3 \right], a_2 \right] \ , && \mathcal{C}_{11} = \left[\left[\left[c, a_3 \right] a_2 \right], a_1 \right] \ . &&
\end{aligned} \qquad (116)
$$

Computing the quantum amplitude requires knowing the color traces. These traces can be organized into a symmetric matrix:

Diagonal terms:

$$\begin{aligned}
&\mathrm{Tr}\,\mathcal{C}_1\mathcal{C}_1^\dagger = C_R^4 D_R\,,\\
&\mathrm{Tr}\,\mathcal{C}_2\mathcal{C}_2^\dagger = \mathrm{Tr}\,\mathcal{C}_3\mathcal{C}_3^\dagger = \mathrm{Tr}\,\mathcal{C}_4\mathcal{C}_4^\dagger = \mathrm{Tr}\,\mathcal{C}_5\mathcal{C}_5^\dagger = \mathrm{Tr}\,\mathcal{C}_6\mathcal{C}_6^\dagger = C_A C_R^3 D_R\,,\\
&\mathrm{Tr}\,\mathcal{C}_7\mathcal{C}_7^\dagger = \mathrm{Tr}\,\mathcal{C}_8\mathcal{C}_8^\dagger = \mathrm{Tr}\,\mathcal{C}_9\mathcal{C}_9^\dagger = \mathrm{Tr}\,\mathcal{C}_{10}\mathcal{C}_{10}^\dagger = C_A^2 C_R^2 D_R\,,\\
&\mathrm{Tr}\,\mathcal{C}_{11}\mathcal{C}_{11}^\dagger = C_A^3 C_R D_R\,.
\end{aligned} \tag{117}$$

Diagrams with 0:

$$\begin{aligned}
&\mathrm{Tr}\,\mathcal{C}_1\mathcal{C}_7^\dagger = \mathrm{Tr}\,\mathcal{C}_1\mathcal{C}_8^\dagger = \mathrm{Tr}\,\mathcal{C}_1\mathcal{C}_9^\dagger = \mathrm{Tr}\,\mathcal{C}_2\mathcal{C}_5^\dagger = \mathrm{Tr}\,\mathcal{C}_2\mathcal{C}_6^\dagger = \mathrm{Tr}\,\mathcal{C}_2\mathcal{C}_9^\dagger = 0\,,\\
&\mathrm{Tr}\,\mathcal{C}_3\mathcal{C}_6^\dagger = \mathrm{Tr}\,\mathcal{C}_3\mathcal{C}_8^\dagger = \mathrm{Tr}\,\mathcal{C}_5\mathcal{C}_{11}^\dagger = \mathrm{Tr}\,\mathcal{C}_6\mathcal{C}_{11}^\dagger = \mathrm{Tr}\,\mathcal{C}_7\mathcal{C}_{10}^\dagger = \mathrm{Tr}\,\mathcal{C}_8\mathcal{C}_{10}^\dagger = 0\,.
\end{aligned} \tag{118}$$

Traces involving the "Wheel" diagram (see Appendix D):

$$\begin{aligned}
&\mathrm{Tr}\,\mathcal{C}_1\mathcal{C}_{10}^\dagger = \mathrm{Tr}\,\mathcal{C}_2\mathcal{C}_{11}^\dagger = \mathrm{Tr}\,\mathcal{C}_5\mathcal{C}_6^\dagger = \mathrm{Tr}\,\mathcal{C}_7\mathcal{C}_8^\dagger = W - \tfrac{1}{8}C_A^3 C_R D_R\,,\\
&\mathrm{Tr}\,\mathcal{C}_1\mathcal{C}_{11}^\dagger = \mathrm{Tr}\,\mathcal{C}_2\mathcal{C}_{10}^\dagger = \mathrm{Tr}\,\mathcal{C}_5\mathcal{C}_8^\dagger = \mathrm{Tr}\,\mathcal{C}_6\mathcal{C}_7^\dagger = -W + \tfrac{1}{8}C_A^3 C_R D_R\,.
\end{aligned} \tag{119}$$

Remaining off-diagonal terms:

$$\begin{aligned}
&\mathrm{Tr}\,\mathcal{C}_1\mathcal{C}_2^\dagger = -\tfrac{1}{2}C_A C_R^3 D_R\,,\\
&\mathrm{Tr}\,\mathcal{C}_1\mathcal{C}_3^\dagger = \mathrm{Tr}\,\mathcal{C}_1\mathcal{C}_5^\dagger = -\tfrac{1}{2}\left(C_R - \tfrac{1}{2}C_A\right)C_A C_R^2 D_R\,,\\
&\mathrm{Tr}\,\mathcal{C}_1\mathcal{C}_4^\dagger = \mathrm{Tr}\,\mathcal{C}_1\mathcal{C}_6^\dagger = -\tfrac{1}{2}\left(C_R - \tfrac{1}{2}C_A\right)^2 C_A C_R D_R\,,\\
&\mathrm{Tr}\,\mathcal{C}_2\mathcal{C}_3^\dagger = \mathrm{Tr}\,\mathcal{C}_2\mathcal{C}_7^\dagger = \mathrm{Tr}\,\mathcal{C}_3\mathcal{C}_4^\dagger = \mathrm{Tr}\,\mathcal{C}_3\mathcal{C}_9^\dagger = -\tfrac{1}{4}C_A^2 C_R^2 D_R\,,\\
&\mathrm{Tr}\,\mathcal{C}_2\mathcal{C}_4^\dagger = \mathrm{Tr}\,\mathcal{C}_2\mathcal{C}_8^\dagger = \mathrm{Tr}\,\mathcal{C}_3\mathcal{C}_{10}^\dagger = \mathrm{Tr}\,\mathcal{C}_4\mathcal{C}_5^\dagger = \mathrm{Tr}\,\mathcal{C}_5\mathcal{C}_9^\dagger = \mathrm{Tr}\,\mathcal{C}_5\mathcal{C}_{10}^\dagger = -\tfrac{1}{4}\left(C_R - \tfrac{1}{2}C_A\right)C_A^2 C_R D_R\,,\\
&\mathrm{Tr}\,\mathcal{C}_3\mathcal{C}_5^\dagger = \left(C_R - \tfrac{1}{2}C_A\right)C_A C_R^2 D_R\,,\\
&\mathrm{Tr}\,\mathcal{C}_3\mathcal{C}_7^\dagger = \mathrm{Tr}\,\mathcal{C}_4\mathcal{C}_9^\dagger = -\mathrm{Tr}\,\mathcal{C}_5\mathcal{C}_7^\dagger = -\mathrm{Tr}\,\mathcal{C}_6\mathcal{C}_8^\dagger = \tfrac{1}{2}C_A^2 C_R^2 D_R\,,\\
&\mathrm{Tr}\,\mathcal{C}_3\mathcal{C}_{11}^\dagger = \mathrm{Tr}\,\mathcal{C}_4\mathcal{C}_7^\dagger = \mathrm{Tr}\,\mathcal{C}_7\mathcal{C}_9^\dagger = \mathrm{Tr}\,\mathcal{C}_7\mathcal{C}_{11}^\dagger = -\tfrac{1}{8}C_A^3 C_R D_R\,,\\
&\mathrm{Tr}\,\mathcal{C}_4\mathcal{C}_6^\dagger = \left(C_R - \tfrac{1}{2}C_A\right)^2 C_A C_R D_R\,,\\
&\mathrm{Tr}\,\mathcal{C}_4\mathcal{C}_8^\dagger = \mathrm{Tr}\,\mathcal{C}_4\mathcal{C}_{10}^\dagger = -\mathrm{Tr}\,\mathcal{C}_6\mathcal{C}_9^\dagger = -\mathrm{Tr}\,\mathcal{C}_6\mathcal{C}_{10}^\dagger = \tfrac{1}{2}\left(C_R - \tfrac{1}{2}C_A\right)C_A^2 C_R D_R\,,\\
&\mathrm{Tr}\,\mathcal{C}_4\mathcal{C}_{11}^\dagger = -\mathrm{Tr}\,\mathcal{C}_8\mathcal{C}_9^\dagger = -\mathrm{Tr}\,\mathcal{C}_8\mathcal{C}_{11}^\dagger = \tfrac{1}{4}C_A^3 C_R D_R\,,\\
&\mathrm{Tr}\,\mathcal{C}_9\mathcal{C}_{10}^\dagger = \left(C_R - \tfrac{1}{2}C_A\right)C_A^2 C_R D_R\,,\\
&\mathrm{Tr}\,\mathcal{C}_9\mathcal{C}_{11}^\dagger = -\mathrm{Tr}\,\mathcal{C}_{10}\mathcal{C}_{11}^\dagger = \tfrac{1}{2}C_A^3 C_R D_R\,.
\end{aligned} \tag{120}$$

D The Color "Wheel" Diagrams

In the case of three scattering centers some nontrivial color factors appear for the first time in eq. (119). They correspond diagrammatically to the "wheel" diagrams shown in Fig. 10.

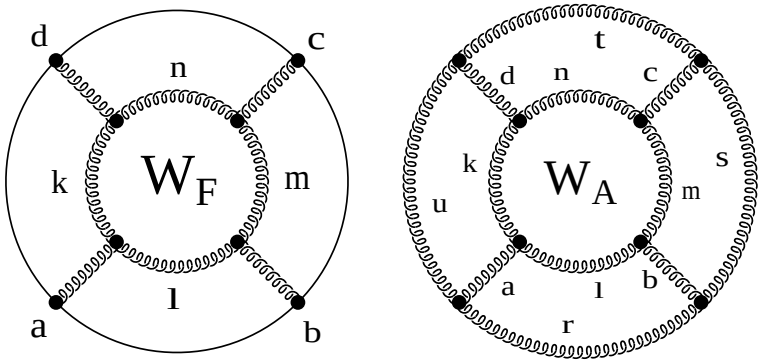

Fig. 10. The "wheel" diagram in the fundamental and the adjoint representations.

For the fundamental representation

$$\{T_a, T_b\} \;=\; \frac{1}{N}\delta_{ab} + d_{abc}T_c \;, \tag{121}$$

It is useful to introduce the complex tensor

$$h_{abc} = d_{abc} + i f_{abc} \;, \quad h_{abc} = h_{bca} = h_{cab} \;, \quad h_{aab} = 0 \;. \tag{122}$$

If the physical case of $SU(3)$, we find

$$\begin{aligned} W_F \;&=\; \mathrm{Tr}\,(T_aT_bT_cT_d)\, f_{kal}f_{lbm}f_{mcn}f_{ndk} = \left(\frac{1}{12}\delta_{ab}\delta_{cd} + \frac{1}{8}h_{abr}h_{rcd}\right)\times \\ &\times\frac{1}{4}\left(5\delta_{ab}\delta_{cd} + \delta_{ac}\delta_{bd} + 5\delta_{ad}\delta_{bc} - 6d_{acr}d_{rbd}\right) = \frac{33}{2} \end{aligned} \tag{123}$$

for the fundamental representation and

$$\begin{aligned} W_A \;&=\; (f_{kal}f_{lbm}f_{mcn}f_{ndk})(f_{rau}f_{udt}f_{tcs}f_{sbr}) = \\ &=\; \frac{1}{4}\left(5\delta_{ab}\delta_{cd} + \delta_{ac}\delta_{bd} + 5\delta_{ad}\delta_{bc} - 6d_{acr}d_{rbd}\right)\times \\ &\quad\times\frac{1}{4}\left(5\delta_{ad}\delta_{cb} + \delta_{ac}\delta_{bd} + 5\delta_{ab}\delta_{dc} - 6d_{acr}d_{rdb}\right) = 189 \;. \end{aligned} \tag{124}$$

for the adjoint representation.

N_c	2	3	4	5
W_F	$\frac{9}{4}$	$\frac{33}{2}$	$\frac{135}{2}$	$\frac{405}{2}$
W_A	24	189	840	2775

Table 1. The N_c dependence of the wheel diagram to be found numerically.

References

[1] J.D. Bjorken, Fermilab-Pub-82/59-THY (1982) and erratum (unpublished).

[2] M. H. Thoma and M. Gyulassy, Nucl. Phys. B **351** (1991) 491.

[3] M. Gyulassy and M. Plümer, Phys. Lett. B **243** (1990) 432.

[4] M. Gyulassy, M. Plümer, M.H. Thoma and X.-N. Wang, Nucl. Phys. A **538** (1992) 37c.

[5] X.-N. Wang and M. Gyulassy, Phys. Rev. Lett. **68** (1992) 1480.

[6] J.F. Gunion and G. Bertsch, Phys. Rev. D **25** (1982) 746.

[7] S.J. Brodsky and P. Hoyer, Phys. Lett. B **298** (1993) 165.

[8] M. Gyulassy and X.-N. Wang, Nucl. Phys. B **420** (1994) 583.

[9] R. Baier, Yu.L. Dokshitzer, A.H. Mueller, S. Peigné, D. Schiff, Nucl. Phys. B **483** (1997) 291.

[10] L.D. Landau and I.J. Pomeranchuk, Dolk. Akad. Nauk. SSSR **92** (1953) 92; A.B. Migdal, Phys. Rev. **103** (1956) 1811; E.L. Feinberg and I.J. Pomeranchuk, Suppl. Nuovo. Cimento **3** (1956) 652; Phys. JETP **23** (1966) 132.

[11] D.W. Dong and M. Gyulassy, Phys. Rev. E **47** (1993) 2913.

[12] M. Gyulassy, P. Lévai, and I. Vitev, in preparation; preliminary numerical results presented at RHIC Winter Workshop, Jan 7-9, 1999, LBNL, see *http* : *//sseos.lbl.gov/ nxu/workshop/talk*06*/ppframe.html*

[13] X.-N. Wang and M. Gyulassy, Phys. Rev. D **44** (1991) 3501; X.-N. Wang, Comp. Phys. Comm. **83** (1994) 307.

[14] T. Sjöstrand, Comput. Phys. Commun. **27** (1982) 243.

[15] U.A. Wiedemann and M. Gyulassy, hep-ph/9906257, submitted to NPB.

[16] B.G. Zhakharov, JETP Letters **63** (1996) 952; *ibid.* **65** (1997) 615.

[17] R. Baier, Yu.L. Dokshitzer, A.H. Mueller, S. Peigné, D. Schiff, Nucl. Phys. B **484** (1997) 265; Nucl. Phys. B **531** (1998) 403; Phys. Rev. C **58** (1998) 1706.

[18] M. Gyulassy, P. Lévai, I. Vitev, *Jet quenching in thin plasmas*, hep-ph/9907343, to appear in Nucl. Phys. A.

[19] R. Field, *Applications of Perturbative QCD*, Addison-Wesley, 1989.

[20] T. Sjöstrand and M. van Zijl, Phys. Rev. D **36** (1987) 2019; T. Sjöstrand, Comp. Phys. Commun. **39** (1986) 347; T. Sjöstrand and M. Bengtsson, *ibid.* **43** (1987) 367.

[21] X.-N. Wang and M. Gyulassy, Phys. Rev. D **45** (1992) 844.

[22] J.P. Blaizot and L. McLerran, Phys. Rev. D **34** (1986) 2739.

[23] M. Rammerstorfer, U. Heinz, Phys. Rev. D **41** (1990) 306.

[24] M. Gyulassy, Y. Pang, and B. Zhang, Nucl. Phys. A **626** (1997) 999.

[25] P. Cvitanovic, Phys. Rev. D **14** (1976) 1536.